Article:
Liu, G, Jiang, Y and Wang, X (2015) Tailoring Particle Microstructures Via Supercritical CO2 Processes for Particular Drug Delivery. Current Pharmaceutical Design, 21 (19). pp. 2543-2562. ISSN: 1873-4286

https://doi.org/10.2174/1381612821666150416101116#sthash.ghBUkP32.6hC84yHv.dpuf

Review paper for ***Current Pharmaceutical Design***

Tailoring Particle Microstructures via Supercritical CO_2 Processes for Particular Drug Delivery

Guijin Liu[1], Yanbin Jiang[1]*, X. Wang[2]

[1] School of Chemistry and Chemical Engineering, South China University of Technology, Guangzhou 510640, China

[2] Institute of Particle Science and Engineering, School of Process, Environmental and Materials Engineering, University of Leeds, Leeds LS2 9JT, UK

* Corresponding author:

Yanbin Jiang

Tel: +86-20-8711-2051

E-mail address: cebjiang@scut.edu.cn (Y. Jiang)

Graphical abstract

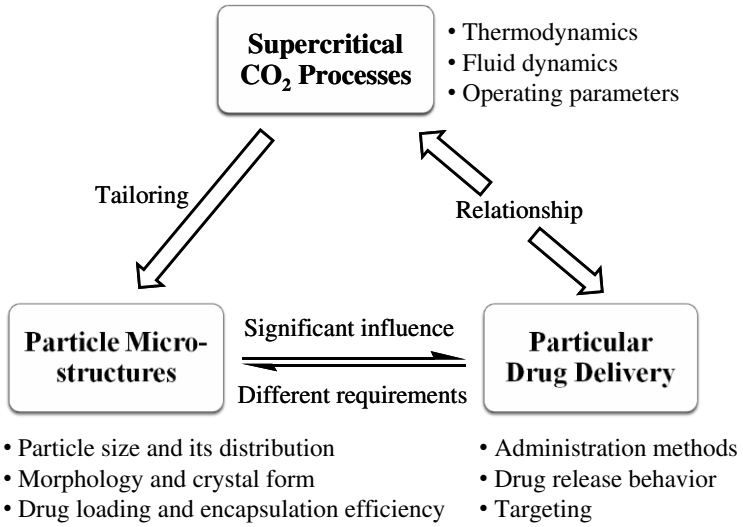

Abstract

Strategies for a particular drug delivery are always of great interest for the pharmaceutical industry, and efficient methods of preparing products with controlled particle microstructures are fundamental for the development and application of drug delivery. Supercritical fluid particle design (SCF PD) processes, as a green and effective alternative to traditional methods, have been effectively employed to produce particles with designated microstructures.

Combining with research experiences in our research group, this review aims to provide a theoretical framework of SCF PD for particular drug delivery. For any drug delivery formulations, macroscopic properties are directly influenced by the particle microstructures, "Inverse" strategies are introduced at first to obtain the needed particle microstructures for a particular drug delivery in this paper. Then, how to produce particles with designated microstructures via SCF PD processes is discussed, mainly focus on the screening and selection of operating parameters according to thermodynamics and fluid dynamics study. Recent examples of SCF micronization and co-precipitation/ encapsulation processes are also summarized with an emphasis on how to tailor the particle microstructures by controlling the operating parameters. Finally, challenges and issues needed further study are briefly suggested for SCD PD.

Keywords: Supercritical fluids, drug delivery, particle design, microstructures, process, operating parameters, thermodynamics, fluid dynamics

1. INTRODUCTION

Strategies for effective drug delivery are always of great interest for the pharmaceutical industry [1], especially the delivery of particular drugs with poor solubility, tissue damage on extravasation, rapid breakdown of the drug in vivo, unfavorable pharmacokinetics, poor biodistribution and lack of selectivity for target tissues [2-4].

Drug delivery process includes the administration of the therapeutic product, the release of the active ingredients by the product, and the subsequent transport of the active ingredients across the biological membranes to the site of action [5, 6]. For a particular drug delivery, macroscopic properties, such as the administration methods, drug release and targeting are determined according to the drug properties and its application. These macroscopic properties are directly influenced by the particle microstructures, such as morphology, particle size (PS), particle size distribution (PSD), crystal form, drug loading (*DL*) and encapsulation efficiency (*EE*) [7, 8]. Thus, the efficient methods of preparing products with controlled particle microstructures are fundamental for the development and application of any drug delivery formulations.

York [9] indicated that an ideal particle formation process for the pharmaceutical industry should be clean, environmentally responsible, single-step operation producing particles with targeted properties. Supercritical fluid (SCF) processes, as an alternative strategy of traditional technologies, provide an attractive platform to achieve these aims and show great promise in particle design [10, 11]. As the most popular SCF, supercritical CO_2 ($scCO_2$) is safe, inexpensive, readily available, and an ideal substitute for many hazardous and toxic solvents. By controlling the level of pressure (*P*), temperature (*T*), or modifier, $scCO_2$ dissolves a broad range of compounds, both polar and non-polar. At present, $scCO_2$ process is one of the fastest growing technologies being adopted by the pharmaceutical industry [12].

As noted by Elvassore and Kikic [13], the concepts of "clean or green chemistry" and "sustainable technology" are of great help to make pharmaceutical industrial applications of SCF processes closer than ever. SCF processes and their fundamentals have been discussed in many reviews, these reviews mainly focus in the use of SCF processes for different pharmaceuticals applications, and occasionally for modeling or fundamentals of these processes [14-16]. Combining with research experiences in our laboratory, this review aims to provide a theoretical framework of SCF particle design (SCF PD) for particular drug delivery.

An overall view of SCF PD for particular drug delivery is shown in Fig.1. “Inverse” strategies are introduced at first to establish the relationship between particular drug delivery and particle microstructures. Then, tailoring particle microstructures via a suitable SCF processes is discussed with an emphasis on the screening and selection of operating parameters according to thermodynamics and fluid dynamics study. Typical examples of SCF micronization and co-precipitation/encapsulation processes for particular drug delivery are summarized.

2. BASIC REQUIREMENTS OF PARTICULAR DRUG DELIVERY

For all particular drug delivery, the administration methods of the therapeutic product should be determined at first, drugs are introduced into the human body by various routes [5, 17], where the selection of these administration methods depends on the disease, the effect desired and the product available [18]. The most common administration methods with their advantages and disadvantages are listed in Table 1. Every administration method has certain requirements on particle microstructures, especially on PS [19-23]. Generally, for oral administration, there is a wide PS range, which tends to be within 0.1-100 μm, according to their gastrointestinal dissolution and absorption characteristics. For injection, the particles in the intravenous solution are distributed to various organs depending on PS. Particles larger than 7 μm are trapped in the lungs, and those smaller than 0.1 μm accumulate in the bone marrow. Those with diameter between 0.1 and 7 μm are taken up by the liver and the spleen. For transdermal administration, particles greater than 10 μm remain on the skin surface; particles between 3-10 μm concentrate in the hair follicles; particles smaller than 3 μm may penetrate both the follicles and stratum corneum. PS also exerts a significant influence on pulmonary drug delivery. Particles with mass median aerodynamic diameter ranging from 1-5 μm, are deposited in the bronchial and alveolar regions predominantly by sedimentation, and have the best pulmonary penetration.

For most particular drug delivery, the drug release behaviors should also be considered. Although vesicles or drug macromolecule conjugates may prolong release, optimal control is afforded if the drug is placed in a polymeric material [24]. Polymeric materials generally release drugs by the following mechanisms [25]: (i) diffusion, (ii) chemical reaction, or (iii) solvent activation. There are two types of diffusion-controlled systems: reservoirs (Fig. 2 A) and matrices (Fig. 2 B). Chemical control is accomplished either by polymer degradation (Fig. 2 C) or chemical

cleavage of the drug from a polymer (Fig. 2 D). Solvent activation involves either swelling of the polymer (Fig. 2 E) or osmotic effects (Fig. 2 F and G).

These drug release mechanisms depend on a number of parameters [26]. Some of them are external, such as concentration of the active substance and carrier in the surrounding medium, pH, and enzymatic action. However, most of them are particle microstructures, such as PS, morphology, crystal form, *DL*, etc. The quantitative interpretation of the values, which obtained in the dissolution assay, is facilitated by the usage of a generic equation, where the equation mathematically translates the dissolution curve in function of some parameters related with the particle microstructures. There are number of kinetic models, which described the overall release of drug from the dosage forms [27]. These methods are classified into three categories: (a) statistical methods, e.g. exploratory data analysis method, repeated measures design, multivariate approach and multivariate analysis of variance [28, 29]; (b) model dependent methods, e.g. zero order, first order, Higuchi, Korsmeyer-Peppas model, Hixson Crowell, Baker-Lonsdale model and Weibull model [30, 31]; and (c) model independent methods [32, 33].

Conventional forms of drugs normally medicate the whole body, reaching healthy areas as well as diseased. Thus, for some particular drug delivery, the transport of the active ingredients to the site of action should be taken into account. Targeted drug delivery refers to predominant drug accumulation within a target zone, which is independent of the method and route of drug administration [34]. The following advantages of drug targeting are evident [35-37]: (a) drug administration protocols may be simplified; (b) drug quantity required to achieve a therapeutic effect may be greatly reduced as well as the cost of therapy; (c) drug concentration in the required sites can be sharply increased without negative effects on non-target compartments. There are a number of parameters that are important for the successful development and manufacturing of targeted drug delivery. The targeting of drugs may be viewed on two levels: (a) organ targeting and (b) cellular targeting. The organ targeting is actually dependent on the size, shape and material properties of the carrier employed, whereas the cellular targeting depends upon a more specific interaction at a molecular level between the carrier and the cellular target. Thus, the targeted delivery systems have significant requirements on particle microstructures. For example, surface properties of nontargeted drug delivery vehicles affect the particle uptake, where the size of the nanoparticles affects their movement in and out of the vasculature, whereas the margination of particles to vessel wall is impacted by their

shape, as shown in Fig. 3 [38].

3. SUPERCRITICAL FLUID PARTICLE DESIGN

Generally, SCF PD processes are classified into three major methods [39], i.e., rapid expansion of supercritical solution (RESS), particles from gas-saturated solution (PGSS) process, supercritical antisolvent (SAS) process. Table 2 lists their various modifications, which depends on whether the $scCO_2$ used as a solvent, a solute or an antisolvent. As well known, knowledge about these processes is of great help to the selection of a suitable SCF process for a particular drug delivery.

3.1 SCF PD Processes and Their Modifications

RESS was patented in 1986 [40], and exploits the ability of the $scCO_2$ to solubilize different compounds. The advantages of RESS include that it is a simple process, and is relatively easy to implement on a small scale. However, the main drawback that limits the scaling of this process is represented by great SCF/solution rate requirement, since the poor solubility of most pharmaceutical products in $scCO_2$. Usually, the solubility value for obtaining a reasonable yield should be on the order of 10^{-4} mole fraction. Therefore, several modifications have been implemented for the RESS process, including RESS into a liquid solvent (RESOLV) [41], RESS into an aqueous solution (RESSAS) [42], RESS-non-solvent (RESS-N) process [43], RESS with solid cosolvent (RESS-SC) [44-46], pre-filtration RESS (PF-RESS) [47], etc. Recently, these RESS processes were specified by Türk [48].

PGSS process uses the property of CO_2 can be solubilised in large quantities in a liquid or a melted solid [49]. The advantages of the PGSS process are similar to those of RESS. These processes perform the production of solvent-free material, as there is no need of organic solvents. Further advantages of the PGSS process are low consumption of CO_2 and a wide range of potential applications, since the solubility of compressed gases in liquids and solids is often high. Particularly, PGSS process is potentially adaptable to protein and lipid processing, and is properly applied to materials with low melting points. Nevertheless, the different physicochemical properties of proteins and lipids may result in large and inhomogeneous particles. Thus, Salmaso et al [50] developed a novel supercritical gas-assisted melting atomization process (GAMA process) to produce the solid lipid submicron particles. GAMA process improved the atomization of PGSS process by using a second gas in the atomization and precipitation vessel. The PGSS process can also be used to

produce particles from aqueous solutions. PGSS-drying is the most used PGSS variation, which was developed by Meterc et al [51] for drying of aqueous green tea extracts. Compared with spray-drying, PGSS-drying provides an inert atmosphere avoiding the possibility of the oxidation. Moreover, PGSS-drying allows drying the solutions with a reduced thermal degradation or contamination of the product, because PGSS-drying is carried out in a closed system, and only the static mixer section of the process operates at high *T*.

SAS is devised to precipitate solid compounds that are not soluble in SCF. Many variations of the SAS technique exist, including the gas antisolvent (GAS) recrystallization, aerosol solvent extraction systems (ASES) and precipitation with compressed antisolvent (PCA) process. GAS is a batch process and the earliest SAS technology, which was proposed in 1989 by Gallagher et al [52]. ASES and PCA are semi-continuous processes, which are devised based on the concept of the GAS. GAS process is simple and particularly useful for the crystallization of sensitive materials, e.g. pharmaceuticals, biological products, explosives, etc, since it operates at moderate *T* [53]. However, a clear disadvantage of GAS process is the lack of effective control on the particle formation. Problems also exist in GAS process, such as exothermic impact during the addition of SCF into solvent or solution. Main advantage of PCA and ASES over GAS is their suitability for continuous operation, which is prerequisite for large scale mass production of particles. To some degree, SAS processes usually means ASES or PCA in many researches. In PCA and ASES, to minimize particle agglomeration frequently observed and to reduce or eliminate drying times, increased mass-transfer rates are required. This has been successfully achieved in the solution enhanced dispersion by SCF (SEDS) process [54], which uses a coaxial nozzle design with a mixing chamber. In addition, to obtain ultrafine particles with narrow size distribution, He et al [55, 56] used SEDS with prefilming atomization (SEDS-PA) process. The principle involved in SEDS-PA is to drive the liquid atomized along a surface as a film within the nozzle, and consequently reaching at the atomizing edge. Besides, the SAS with enhanced mass transfer (SAS-EM) technique, conceived by Chattopadhyay and Gupta [57], utilizes a deflecting surface that vibrates at ultrasonic frequencies to enhance the atomization of the solution.

3.2 Screening and Selection of Operating Parameters

As mentioned above, RESS can be used with scCO_2-soluble molecules, PGSS can be used with CO_2-dissolved molecules, while SAS can process nonsoluble

molecules. For a particular drug delivery, a suitable method is selected based on the drug properties. However, there are many operating parameters for SCF PD processes that have great influence on particle microstructures, as shown in Table 2. Study about the complicated mechanism of particle formation and growth is essential to screening and selection of the operating parameters for producing particles with designated microstructures.

For modeling of SCF processes, a general dynamic equation for simultaneous nucleation, condensation and coagulation is implemented, as described in Eq. (1) [58, 59].

$$\begin{aligned}\frac{\partial n}{\partial t} &= \underbrace{J\left(v^*\right)\delta\left(v-v^*\right)}_{\text{nucleation}} \underbrace{-\frac{\partial\left(Gn\right)}{\partial v}}_{\text{consdensation}} \\ &\underbrace{+\frac{1}{2}\int_0^v \beta\left(v-\bar{v},\bar{v}\right)n\left(v-\bar{v},t\right)n\left(\bar{v},t\right)d\bar{v}}_{\text{coagulation}} \underbrace{-n\left(v,t\right)\int_0^\infty \beta\left(v,\bar{v}\right)n\left(\bar{v},t\right)d\bar{v}}_{\text{coagulation}}\end{aligned} \tag{1}$$

where n denotes the PSD function, t is the time, J is the nucleation rate, v is the particle volume, v^* is the critical volume, δ is the standard Dirac function, G is the condensation growth rate, β is the Brownian coagulation coefficient. Furthermore, it is worthy to notice that the driving force of nucleation and crystal growth for all SCF processes is the solution supersaturation (S), which is a measurement of the difference of solute concentration between the composition of the fluid (y), and the saturation composition (y_{eq}), defined as Eq.(2) [60].

$$S = \frac{y}{y_{\text{eq}}} \tag{2}$$

Based on the S value, the particle nucleation and growth kinetics can be established. By means of the classical nucleation theory, the nucleation rate J, the critical nucleus size r^* and the number concentration of critical nuclei N^* for homogeneous nucleation are given by Eqs. (3-5), respectively [60].

$$J = \Theta\kappa\alpha_{\text{c}}n_{\text{s}}\pi r^{*2}cn_{\text{s}}\exp\left(\frac{-\frac{4}{3}\pi\sigma r^{*2}}{k_BT}\right) \tag{3}$$

$$r^* = \frac{2\sigma v^s}{k_BT\left(\ln S\right)} \tag{4}$$

$$N^* = N_2 \cdot \exp\left\{-\frac{16\pi}{3}\left(\frac{\sigma\left(v^s\right)^{2/3}}{k_B T}\right)^3\left(\frac{1}{\ln S}\right)^2\right\} \tag{5}$$

where, Θ is the non-isothermal factor, κ is the Zeldovich nonequilibrium factor, α_c is the condensation coefficient, n_s is the number of condensable molecules, c is the mean thermal velocity, σ is the solid-fluid interfacial tension, k_B is the Boltzmann's constant and v^S is the solid molecular volume. After nucleation, the particle assumes to grow up until S disappears. The growth of the particles could be governed by the diffusion where the diffusion coefficient of the solute in the dense fluid can be calculated from the Stokes-Einstein equation. The growth rate of particle diameter with t thus may be estimated as given below [61].

$$\frac{\mathrm{d}D_\mathrm{p}}{\mathrm{d}t} = \frac{2D_\mathrm{C}v^s N^*}{D_\mathrm{p}} Q$$
$$\text{where } Q = \frac{1+K_n}{1+1.71K_n+1.333{K_n}^2} \tag{6}$$

where D_p is the diameter of the particles, K_n is the Knudsen number, and D_C is the diffusion coefficient of the solute in a SCF as follows.

$$D_\mathrm{C} = 7.4\times10^{-5}\frac{TM^{0.5}}{\mu\cdot {v^s}^{0.6}} \tag{7}$$

where M is the solvent molecular weight and μ is the pure solvent viscosity.

Thus, S is a key factor to determine the product quality, especially the particle microstructures. In general, high S cause fast nucleation and crystal growth, therefore a larger number of smaller particles are produced when S is increased. As shown in Fig. 4, S is controlled by the thermodynamics and fluid dynamics, which are influenced by operating parameters, such as T, P, solvent, nozzle design, flow rate, etc. Therefore, to establish the relationship between operating parameters and particle microstructures, it is of great importance to get a rational understanding of the thermodynamics and fluid dynamics.

3.2.1 Thermodynamics study

In a SCF process, thermodynamics is mainly focuses on the study of the solubility of the substance in CO_2 at high P, maybe with some amount of organic solvents. This is vital for setting operating parameters, e.g., T, P and organic solvents. Solute solubility data in the SCF can be collected from the literature when they exist, or be obtained from experiments or modeling. Solubility data for 783 different compounds published from the early 1960s to 2004 are presented by Gupta et al [62].

Solubility data for solid compounds in sub- and supercritical fluids reported in the literature between 2005 and 2010 are summarized by Škerget et al [63]. However, most of these data are for binary systems, solubility data for ternary and multicomponent systems are still limited. Various methods to measure solubility in SCF can be divided into two major categories, i.e. static and dynamic [62-64]. For example, the supercritical phase behaviors of the poly(lactic acid)/poly(ethylene glycol)/poly(lactic acid) (PLLA-PEG-PLLA) + CO_2 + dichloromethane (DCM) system and the PLLA-PEG-PLLA + CO_2 + DCM + Ethanol (EtOH) system were investigated using the static method [65]. The effects of *T*, the mass fraction of DCM (or DCM + EtOH) (*w*), the PEG mass fraction (*f*) in PLLA-PEG-PLLA on cloud-point *P* were shown in Fig. 5.

The solubility of a pure solid component in a SCF can be expressed as a function of the operating *P* and *T*. However, the calculation of phase equilibrium at high *P* presents several peculiarities: (a) many methods originally developed for low *P* calculations, are not applicable at high *P*; (b) the behavior of the fluid can be strongly affected by the presence of a component at near-critical conditions; and (c) the mixtures of interest frequently include components with large differences in molecular weight or polarity. Models for supercritical-phase equilibriums fall into several categories. The most common method treats the SCF phase as a dense gas, and uses an equation of state (EOS) to calculate the fugacity coefficient of the solute in the fluid phase, e.g., the Peng-Robinson (PR) equation (Eq. (8)) [66, 67].

$$P = \frac{RT}{v - b} - \frac{a}{v(v - b) + b(v - b)} \tag{8}$$

This type of equations establishes a relation between *P*, *T* and molar volume (*v*). In order to take into account the non-ideal behaviour, energetic parameters (*a*) and covolume (*b*) must be introduced. There are also a large number of semiempirical correlations, such as the Chrastil's equation (Eq. (9)) [68, 69].

$$y = \rho_1^c \exp(\frac{A}{T} + B) \tag{9}$$

Eq. (9) is based on the solvate complex formed between solute and SCF at equilibrium, proposing a relation between *y* and the density of the SCF (ρ_1). It can be seen that three parameters (*e*, *A* and *B*) must be determined for Eq. (9) by regressing experimental against theoretical data.

Based on thermodynamic study, phase diagrams can be depicted to decide the process paths of various SCF processes. The most applicable phase diagram for the binary solid-scCO_2 systems in RESS and PGSS is shown in Fig. 6 [70, 71]. The

solid-liquid-vapor (S-L-V) lines intersect with the critical lines (L=V) at two distinguished point, i.e. the lower critical end point (LCEP) and the upper critical end point (UCEP). For RESS, depending on the pre-expansion and expansion of *P* and *T*, the expansion trajectory may cross the V-L line of CO_2, thus leading to the formation of liquid CO_2 droplets. In some cases, the expansion path may even intersect the S-L line of the diagram, so CO_2 snow is produced, which causes severe safety problems of clogging, especially if CO_2 freezes inside the expansion nozzle. In RESS, therefore, it is important to predict the behavior of the solubility in the SCF near the UCEP, in order to choose *P* and *T* values which give the maximum amount of solute in $scCO_2$ without appearance of a liquid phase. Investigation on the PGSS thermodynamics has been performed by Elvassore et al [72] though calculating the enthalpy changes along the process with the perturbed-hard-sphere-chain-theory EOS. Results indicated that the melting point was found to decrease when increasing *P*, until a minimum in the melting point was reached; afterwards, the melting point was increasing together with *P*. In PGSS, the $P-T$ trace of the S−L−V equilibrium gives information on *P* needed to melt the solute and form a liquid phase at a given *T*, and to calculate its composition.

A simple representative phase diagram of the ternary solid-solvent-SCF systems at constant *T* and *P* is shown in Fig. 7, where dashed arrows represent the process paths of various SCF processes. At *P* above the critical point of the binary organic solvent-SCF mixture, the number of coexisting phases reduces from six to four [73]. About ternary mixtures, which are mostly related to SAS, a phase behavior study of the system is extremely useful to address the feasibility of the process and to exploit the effects of *T* and *P* [74]. Moreover, alternative polymeric particle topography and shapes depended upon process paths followed in the phase diagram were reported. For example, Reverchon et al [75] performed an experimental study on SAS precipitation to gain insight into the role of phase behavior and atomization in controlling morphology and dimension of precipitates. Results showed that operating above the mixture critical point (MCP) of the ternary mixture yttrium acetate/dimethyl sulfoxide (DMSO)/CO_2, sub-micrometric particles were generated nearly independently from the size of the injector and of the apparatus. The results also show that it is possible to modify the particle dimension by simply changing the operating *P* and/or *T* in the vicinity of the MCP. The use of a pseudo-binary diagram *P*-molar fraction has been proposed as a base framework to explain the relationship between the particle morphology and the phase behavior of processed mixtures.

Particularly, it is found that the single-phase region in the gas-rich side of the *P*−composition diagram and below the MCP is usefully explored to modify the particle dimensions of the precipitate.

3.2.2 Fluid dynamics

One of the main aspects of fluid dynamics is the study of jet hydrodynamic, which contributes to the nozzle design and selection of other operating parameters. Nozzle design includes geometry, size, distance and angle of impact against the surface of the jet stream [76].

A schematic of the RESS expansion device is displayed in Fig. 8. From the nozzle exit, the fluid expands as a supersonic free jet followed by another subsonic jet where the jet interacts significantly with the background gas present in the expansion region. These two jet regions are separated by the Mach disk [77]. Referring to Fig. 8, the relation between the jet height $2r$ along the expansion pathway to the Mach disk, with the distance x is expressed as Eq. 10.

$$r = \frac{\left(\left(D_{\text{nozzle}} - D_{\text{M}}\right)/2\right)}{L_{\text{M}}}\left(x - L_{\text{nozzle}}\right) + \frac{D_{\text{nozzle}}}{2} \tag{10}$$

where L_{nozzle} and L_{M} are the length of the nozzle and the length of the supersonic free jet region, respectively, D_{M} denotes the diameter of the Mach disk. The L_{M} and D_{M} can be calculated from the following Eqs. (11) and (12) based on the nozzle diameter D_{nozzle}, pre-expansion pressure P_0 and expansion pressure P_{post}, respectively [78].

$$L_{\text{M}} = 0.67 D_{\text{nozzle}} \sqrt{\frac{P_0}{P_{\text{post}}}} \tag{11}$$

$$D_{\text{M}} = 0.5625 L_{\text{M}} \tag{12}$$

Weber et al [79] studied the influence of the capillary geometry by calculating the PSD resulting from nozzles with different $L_{\text{nozzle}}/D_{\text{nozzle}}$ ratios. As $L_{\text{nozzle}}/D_{\text{nozzle}}$ increases, the major part of the *P* drop is due to friction and is shifted closer to the exit (in normalized distances). Thus, expansions in long capillaries are closer to isenthalpic paths, in contrast to the virtually isentropic paths followed by expansions in short devices. Size distribution of particles generated in long capillaries is generally broader. In expansion devices with high $L_{\text{nozzle}}/D_{\text{nozzle}}$ ratios, bimodal PSD may occur because of the second burst of nucleation. Reverchon et al [80] also demonstrates that for small $L_{\text{nozzle}}/D_{\text{nozzle}}$ orifices a large part of the *P* drop, and almost all *T* decrease associated with RESS take place in the post-expansion chamber. This observation confirms the important role of the process parameters connected to the post-expansion

device. The nozzle needs to be maintained at a suitable pre-expansion T to prevent the premature precipitation of the solute. Some researches use the nozzle T as an additional parameter for the control of particle characteristics, although the influence of this parameter is usually limited [81].

PGSS process has similar jet hydrodynamic with RESS process. The nozzle hydrodynamics of the PGSS process is contained in the papers of Li et al [82, 83] for the CO_2 and hydrogenated palm oil (HPO) system. An annular mist flow at the exit of the nozzle with an existing equilibrium between the CO_2-rich gas phase and the mixed CO_2-HPO liquid phase was considered. The results indicated that at the exit of the nozzle, PSD is narrower with a smaller PS because the particles are formed by melt crystallization, but if the particle formation is due to an atomization process, PSD is larger and wider. In many cases the number percentage of particles produced by the melt crystallization process prevail over that produced by the atomization process. Usually, only high pre-expansion T can produce particles mainly from atomization. The D_{nozzle} has only a negligible effect on the produced PS, but has a more evident effect on PSD. Large D_{nozzle} usually produce unimodal distribution particles.

To study the hydrodynamics of the SAS process, most authors assumed that the jet of organic solvent behaves like a liquid jet injected into a gas. This supposition allows applying the classic theory of jet break-up. The break-up length of the jet is studied and correlated as a function of the Reynolds (Re) and Weber numbers (We), defined as Eqs (13) and (14).

$$Re = \frac{\rho u D_{\text{nozzle}}}{\mu} \tag{13}$$

$$We = \frac{\rho u^2 D_{\text{nozzle}}}{\sigma} \tag{14}$$

where, u is the velocity.

However, three different phenomena can be observed when the solution is injected into $scCO_2$, i.e., (a) jet break-up into rather large droplets (drops), (b) jet atomization into small droplets, and (c) “gas-plume” like mixing, when no droplets are formed, as shown in Fig. 9 [84]. The classic theory of jet break-up is disabled when the jet spreads forming a gas-plume.

To overcome this shortage, Martín et al [85] considered jet hydrodynamics as the mixing of two completely miscible fluids forming a gas-plume, and is modeled with a k-ε turbulence model, which consists of two semi-empirical equations for the turbulent kinetic energy k, and the turbulent kinetic energy dissipation rate ε. Lengsfeld et al [86] developed a method for predicting dynamic surface tension and

combined this method with linear jet breakup equations to accurately predict jet breakup lengths in immiscible to highly miscible systems. For highly miscible systems, they proposed that microparticle formation results from gas-phase nucleation and growth within the expanding plume, rather than by nucleation within discrete liquid droplets.

Furthermore, Reverchon et al [87] proposed a possible formation mechanism of nanoparticles and microparticles, which is based on the competition between two characteristic times: (a) time of jet break-up (τ_{jb}), i.e., the time required to the liquid jet to break at the exit of the nozzle; (b)time of surface tension vanishing (τ_{stv}), i.e., the time required to reduce to near zero the surface tension of the liquid in the SCF mixture formed in the precipitator. The results indicated that if $\tau_{stv} < \tau_{jb}$, nanoparticles formation by "gas to particle" precipitation is observed. Instead, if $\tau_{stv} > \tau_{jb}$, microparticles formation by micrometric droplets drying is the prevailing process. Further explanations of the occurrence of typically produced particle morphologies have been suggested in other works of Reverchon et al [84, 88-90], where the elastic or inelastic in situ light scattering techniques were used to gain direct information about the mechanisms involved in the SAS process.

The formation mechanisms of amorphous nano-, micro-, or expanded micro particles are well analyzed and well understood based on time scale approaches. While, Rossmann et al [91] indicated that this time scale model is not applicable for systems forming crystalline structures. The saturation solubility of the solute in mixtures of solvents and antisolvents was proposed as the indirect classification criterion to distinguish amorphous precipitating or crystallizing. Furthermore, Dowy et al [92] developed an optical method to measure the supersaturation in situ for SAS process. Firstly, saturation mole fractions of the solute were measured via elastic light scattering. Secondly, the actual solute mole fraction was imaged in situ during the injection of the solution into the antisolvent using a Raman based optical measurement technique.

Another aspect of fluid dynamics is the study of mass transfer, especially in SAS processes. Once the droplets have been formed inside the SCF, rapid transfer of CO_2 into these droplets and the solvent out of these droplets causes the droplets to expand rapidly. Werling et al [93] indicated that it is useful to define a droplet radius based on the difference in density between the solvent-rich and the antisolvent-rich regions, because the droplet radius is a key parameter for describing the extent of mass transfer and for determining the effect of process conditions on diffusion. The present mass

transfer model is related to droplet turbulence studies, and a simplified continuity equation for a chemical species is expressed as Eq. (15) [85].

$$\rho\left(u_r\frac{\partial\omega}{\partial r}+u_z\frac{\partial\omega}{\partial z}\right)=-\frac{1}{r}\frac{\partial}{\partial r}\left(rj_r\right)+r \tag{15}$$

where ω is the mass fraction, r is the radial direction, z is the axial coordinate. And j_r is the diffusive flux calculated by simplifying the Maxwell-Stefan equations to the well-known Fick law for binary mixtures, which calculated by Eq. (16).

$$j_r=-\rho D^{\mathrm{T}}\frac{\partial\omega}{\partial r} \tag{16}$$

where D^{T} is the turbulent diffusivity.

Besides, it is worth to note that in the SAS-EM technique, major factors responsible for size reduction are the droplet size reduction due to ultrasonic atomization and the increased mixing due to ultrasonic streaming [94]. The droplet diameter (D) is proportional to the wavelength on the liquid film surface and can be determined as [95].

$$D=0.34\left(\frac{8\pi\sigma}{\rho F^2}\right)^{1/3} \tag{17}$$

where F is the vibration frequency.

4. SCF PD PROCESSES FOR PARTICULAR DRUG DELIVERY

Recently, numerous studies of SCF PD processes have been reported to enhance the solubility of poorly water-soluble drugs, design the sustained release systems, and develop the targeted systems. The typical SCF PD processes for a particular drug delivery are micronization and co-precipitation/encapsulation, as shown in Fig.10.

Micronization processes tailor PS, PSD and morphology of particles to meet the different drug administration methods, improve the bioavailability of pharmaceuticals presented in a solid formulation. Furthermore, micronization processes modify the physical structure of the crystal to obtain the polymorphic or amorphous forms, which might exhibit higher solubility and bioavailability.

Co-precipitation/encapsulation processes produce drug delivery systems (DDS) with anticipated particle microstructures, which effectively improve pharmacological and therapeutic properties of a particular drug by controlling the rate, time and place of release of drugs in the body.

4.1 SCF Micronization Processes

Micronization processes have been gaining increasing importance in particle design to produce particles with suitable microstructures, since PS, PSD, morphology and sometimes even the crystal form of particles produced in different industries are usually not appropriate for the subsequent use. Conventional methods, such as jet and ball milling, spray drying and recrystallization using solvent evaporation or liquid anti-solvent, have the common disadvantage of poor control of PSD. The conventional techniques also face some problems, e.g., thermal and chemical degradation of products, large amounts of solvent use and residues. Different with the conventional techniques, SCF PD offers a simpler and better control process for the development and production of nano- or micro- particle drugs, which easy adapt to the principles of green chemistry and green engineering, as well as the new regulatory system of process analytical technology and quality by design.

4.1.1 Objectives of SCF micronization processes

SCF PD processes have been largely reported to micronize drugs for different delivery purposes, which mainly include the following three objectives.

First, different PS can be produced by one kind of SCF PD processes for a particular drug, which means SCF micronization processes meet the requirements of different drug administration methods, especially the pulmonary drug delivery. For example, Steckel et al [96] micronized 8 different steroids by ASES processes for pulmonary delivery, the results showed that the median PS of the steroid particles was in most cases lower than 5 μm and consequently within the respirable range. Todo et al [97] improve insulin absorption from dry powder after administration in lung, where the dry powders were prepared with or without an absorption enhancer (citric acid) by SAS process. Bakhbakhi et al [98] micronized beclomethasone-17, 21-dipropionate using GAS process, the results showed that the GAS process has the potential to produce steroid with powder properties suitable for inhalation therapy.

Second, SCF micronization processes effectively decrease PS or produce amorphous particles, which enhance the dissolution rate and solubility of poorly water-soluble drugs. For example, Keshavarz et al [99] micronized raloxifene by RESS process, the results showed that raloxifene PS reduced from 45.28 μm to 18.93 nm, and a 7-fold increase in dissolution rate was obtained. Varshosaz et al [100] produced amorphous cefuroxime axetil (CFA) nanoparticles with Z-average PS between 158 and 513 nm by RESS process, the results indicated that more than 90% of the nano-sized CFA formulations were dissolved in 3 min and complete dissolution occurred within 20 min, while the commercial CFA did not achieve complete

dissolution during 60 min of the testing period. Kim et al [101] prepared amorphous atorvastatin calcium nanoparticles with mean PS ranging between 152 and 863 nm using SAS process, the results proved that the dissolution rates were highly increased by the reduction of PS resulting in an increased specific surface area, and the absorption after oral administration to rats was markedly increased.

Third, SCF micronization processes also modify the crystal form of the polymorphic drugs, which might exhibit higher solubility and bioavailability. Bolten et al [102] modified the crystal structure of carbamazepine particles by varying the pre-expansion conditions of RESS, the results demonstrated that C-monoclinic carbamazepine particles were produced at pre-expansion *T* higher than 363 K, while triclinic carbamazepine particles were produced at 333 K and 300 bar. Rossmann [103] crystallized paracetamol particles using SAS process, where the polymorph of paracetamol crystals was adjusted between monoclinic and orthorhombic by varying the content of ethanol in the solution. Using ethanol as the organic solvent, always the monoclinic polymorphic form I of paracetamol was generated irrespectively of the *P* and the concentration. It was also found that already 30% of acetone in the initial mixture is sufficient to change the polymorphic form from monoclinic to orthorhombic. Recrystallzation and micronization of 10-hydroxycamptothecin (HCPT) was investigated using SAS process in our previous study [104], as shown in Fig.11, two different polymorphs were found, the results also indicated that SAS process modified the form of HCPT from monohydrate to anhydrous.

4.1.2 Tailoring particle microstructures via SCF micronization processes

The main objective of SCF micronization processes is to produce micro- and/or nanoparticles with controlled PS, PSD, morphology and crystal form. Some recent reports of SCF micronization processes are exampled in Table 3, which focus on how to tailor the PS by manipulating the operating parameters.

Thermodynamics are considered at first in many studies to guide the formation of drug fine particles. Huang et al [105] determined the solubility of progesterone and correlated the solubility data with three empirical density-based models and the PR EOS model before preparing progesterone fine particles with RESS. Solubility of solute in the $scCO_2$, which is mainly controlled by extraction *T* and *P*, is an important factor for the particle formation in the RESS process, because it is directly related to *S*. The results showed that increased with increasing extraction *P*. Besides, high extraction *T* induces low progesterone concentration as constant extraction *P* is lower than the crossover *P* of 210 bar, but induces high progesterone concentration as

extraction *P* is higher than 210 bar. And small progesterone particles were obtained at high extraction *P* or *T*. Based on the progesterone solubility data, effect of extraction *T* and *P* on the average PS of produced materials are predicted and explained combined with the crystal nucleation rate and growth by coagulation or by condensation after nuclei.

Chen et al [109] employed a modified PGSS process to prepare PEG6000-ibuprofen composite particles after investigating the S-L-V phase equilibrium behavior of the PEG6000-ibuprofen-CO_2 system. Then the composite powder was then dispersed into water to remove PEG6000 and obtain ibuprofen nanoparticles. The results showed that increase of the *P* decreases the melting *T* of the ibuprofen-PEG6000 mixture. According to the thermodynamics data, suitable operating *T* and *P* at different PEG molecular weight were selected, and spherical ibuprofen nanoparticles with diameter of 20-500 nm were prepared at different conditions.

Theophylline microparticles were prepared by Franceschi et al [114] using SAS process, where a mixture of EtOH and DCM was used as solvents. In order to help selecting the appropriate operating conditions and understand the precipitation mechanism, the fluid phase behavior of ternary (CO_2-solvents) and quaternary (CO_2-solvents-theophylline) systems were investigated using a static synthetic method. Phase diagram of the mixture revealed that the contact mechanism between solution and antisolvent occurred in two different ways, which influenced the aggregation, PS and PSD. The results verified that the addition of theophylline to the ternary system consisting of the organic solvents and CO_2 did not influence the transition *P*, which allows the consideration of a ternary system to select the operating points in the phase diagram. PR-EOS demonstrated to be suitable for representing multicomponent systems. The precipitation *T*, flow rate of solution (F_s) and scCO_2 (F_c), and C_d in the solution were the most important variables that affected the precipitation results.

Ultra-fine particles of α-chymotrypsin were produced with SAS technique by Chang et al [115], it was found that the phase behavior of the mixtures during precipitation governed the product's morphology, as shown in Fig. 12. Uniform networked nano-particles were obtained as the precipitation was implemented in the supercritical region. The uniformity of the resulting products became worse when the particles were precipitated around the critical region. Irregular micro-scale aggregated particles were formed in the superheated region, while both dense cake and spherical clusters were produced in the V-L coexistence region.

Fluid dynamics is essential to discuss the influence of flow rate and nozzle design on particle microstructures. Micronization of gemfibrozil particles was carried out using RESS process by Baseri et al [116], where effects of spray distance, nozzle type and nozzle diameter on the characteristics of gemfibrozil particles were studied. The results showed that two competition phenomena for spray distance, i.e., increasing effect (increase of growth time by increasing of spray distance) and decreasing effect (decrease of flow velocity by increase of spray distance) lead to make a maximum value of mean PS in the spray distance of 5.5 cm. Particles produced by capillary nozzle have higher growth time and it results in larger particles in comparison with the orifice nozzle. A larger diameter of nozzle provides only higher total flow rates without bringing about a change of axial velocity, thus it has insignificant effect on the crystallization process.

He et al [55] precipitate ephedrine from ethanol solution using SEDS-PA process, where a prefilming atomizer was designed on the basis of the mechanisms of atomization and applied to the SEDS process. It was found that PS decreases with increasing F_c, because high F_c reinforced the impingement of dense gas on the liquid film, which results in the formation of fine droplets and intense mixing of $scCO_2$ and droplets. With the increase of F_s, PS increased in the beginning, then decreased. When F_s is low and F_c is relatively high, the impingement of the atomizing dense gas on liquid sheet is the main factor of jet breakup in the spray process and the liquid sheet is rapidly disintegrated into droplets as prompt atomization; drop sizes and PS increase with F_s for constant F_c in this case. When F_s is high and F_c is relatively low, the interaction between the liquid and the dense gas is weak and the liquid sheet is disintegrated into drops according to the wavy-sheet mechanism; in this case, PS decrease with F_s for constant F_c.

Micronization of camptothecin (CPT) has been performed using SAS process in our previous study [117]. The results indicated that solvents with higher ρ/μ ratio, lower σ and lower solvation power will form smaller CPT microparticles with lower crystallinity. The possible reason is that higher ρ/μ means the higher *Re* of solution at the nozzle exit, and low σ of the pure liquid shortens the elapsed time of the interface between injected solution and bulk CO_2. These are beneficial to the formation of small droplets or "gas-plume", which provide a larger mass transfer surface between the liquid and the gaseous phase, resulting in a faster *S* of the solute occurring and less time for the particle growth, then forming small particles. On the other hand, at same CPT concentration, the saturation ratio is higher when using solvents with lower

solvation power, and this helps to produce smaller particles.

4.2 SCF Co-precipitation/Encapsulation Processes

The formulation of drugs together with a biocompatible or biodegradable carrier material by co-precipitation/encapsulation processes has a great relevance for pharmaceutical industry. Usually, co-precipitation/encapsulation techniques are divided into three classes: (a) chemical processes like molecular inclusion or interfacial polymerization; (b) physicochemical techniques like coacervation and liposome encapsulation; (c) physical processes like spray drying, co-crystallization, extrusion or fluidized bed coating. However, major advances in drug manufacture have highlighted the limitations of conventional particle formation and pretreatment processes in fine-tuning the characteristics required, since the harsh processing conditions and poor properties of products. The application of SCF PD as an alternative to the conventional processes has been an active field of research and innovation during the past two decades.

4.2.1 Objectives of SCF co-precipitation/encapsulation processes

First, sustained release systems can be designed by SCF co-precipitation/ encapsulation processes. For example, Duarte et al [118] prepared Ethylcellulose/ methylcellulose blends by solvent-evaporation and SAS process. Then, SCF impregnation was performed to prepare naproxen loaded microspheres. The results indicated that microspheres prepared by SAS process have a higher loading capacity and present a slower release profile. The systems studied present a release mechanism controlled by drug diffusion, which complies Fick's law of diffusion.

Lee et al [119] employed a modified SAS-EM process to fabricate controlled-release matrices for Paclitaxel. When ultrasonication was applied, more uniform particles in the submicron size range were obtained. In vitro release studies showed that, at *DL* of 3% or less, almost the entire drug is released during a 1 month period. At higher *DL* (10%), approximately half the drug is released during a 1 month period and subsequent release is very slow. A similar result is obtained at 5% *DL*. This is very likely due to the formation of drug crystals dispersed within the polymer matrix. Similar phenomenon was observed at our previous work [120], where the micronized HCPT is dispersed into the PLLA matrix using SAS process. The result of in vitro drug release test indicated that the crystallinity of HCPT in microparticles affects the control release performance, and the good encapsulated microparticles with higher *DL* and higher crystallinity are better.

10-Hydroxycamptothecin proliposomes (HCPT-PL) were also prepared using the SAS process in our previous study [121], the results showed that spherical or clavate

HCPT-PL were obtained under different *DL*, as shown in Fig. 13. For the optimized HCPT-PL, the residual DCM meets the ICH requirement, and part of the encapsulated HCPT still maintains its crystalline state. The result of in vitro release rate study showed that HCPT-PL sustained the HCPT release rate successfully, where the drug release of the optimized HCPT-PL followed the first order kinetics, and the drug diffusion mainly corresponded to a Fickian diffusion mechanism during the first 10 h.

SCF co-precipitation/encapsulation processes are also employed to produce targeted DDS. One way for achieving targeting of specific cell types is suggested that modifying the carrier materials with the targeting moieties, such as ligands, peptides or aptamers. Among them, folate (FA) is one of the most common targeting moieties, and has been covalently attached to a wide array of drug delivery carriers.

For example, Zu et al [122] prepared FA-dextran-CPT tumor-targeted nanoparticles by SAS process. Under the optimum operation conditions, FA-dextran-CPT nanoparticles with a mean PS of 182.21 nm were obtained, and the *EE* and *LD* were 62.13% and 36.12%, respectively. Compared with other methods for preparing tumor-targeted nanoparticles, the SAS process is uncomplicated to implement. Moreover, Results suggest FA-dextran-CPT nanoparticles have excellent potential in drug delivery systems for cancer chemotherapy.

Zhao et al [123] prepared HCPT-chitosan (HCPT-CS) nanoparticles by the SAS-ionic crosslink combination method; the resulting HCPT-CS nanoparticles were then conjugated with folate for specific targeting. Optimum conditions for preparing desired HCPT-CS nanoparticles with a mean PS of 173.5 nm and entrapment efficiency of 77.3% were obtained. The resulting FA-HCPT-CS nanoparticles reveal that the amount of folate conjugation was 197.64 mg/g CS. FA-HCPT-CS nanoparticles used in drug carrier systems could have potential value in HCPT-sensitive tumors.

Another way for drug targeting is using polymer/magnetite particles, which is based on the attractive forces between the applied magnetic field at the target site and the magnetic material dispersed within the drug-loaded polymer particles. Vezzù et al [124] produced lipid microparticles magnetically active by a modified PGSS process. The *EE* of magnetite nanoparticles was about 30% and increased with the concentration of magnetite in the initial mixture. The possibility to drive these magnetically active particles by an external magnet was demonstrated in a simple apparatus simulating a vessel of the circulatory system. The coating of magnetite nanoparticles with lipids by the modified-PGSS process presently developed provides materials which may be interesting for diagnostic and therapeutic applications.

Chattopadhyay et al [125] used SAS and SAS-EM processes to produce magnetite-encapsulated PLGA, PMMA and Eudragit RS biodegradable polymer particles via co-precipitation of the polymer with a suspension of magnetite particles in mineral oil and a fatty acid surfactant, where DCM is solvent. Chen et al [126] prepared Fe_3O_4-PLLA-PEG-PLLA magnetic microspheres (MMPs) in a process of suspension-enhanced dispersion by supercritical CO_2, a modified SEDS process by employing the "injector"-like suspension delivery system. Methotrexate-loaded Fe_3O_4-PLLA-PEG-PLLA MMPs were produced by co-precipitation and microencapsulation processes. The resulting MMPs had a spherical shape, with a good magnetic response, which would have potential as a sustained and targeted drug delivery system when combined with the microencapsulation process.

4.2.2 Tailoring particle microstructures via SCF co-precipitation/encapsulation processes

Besides PS, PSD, morphology and crystal form, particle microstructures like *DL* and *EE* are essential to be tailored for SCF co-precipitation/encapsulation processes. Table 4 lists recent SCF co-precipitation/encapsulation processes with an emphasis on the effects of operating parameters on PS, *DL* and *EE*. Although a fairly general experimental result of the effects of operating parameters on particle microstructures is not available up to now, some correlations have been proposed and rationally explained on the basis of the thermodynamics and fluid dynamics knowledge.

Typical examples for RESS co-precipitation/encapsulation processes are as follow. Kim et al [134] investigated the effects of fluid phase interactions on particle formation using RESS though combining the solubility data with morphology studies. The solubility of PLLA and naproxen/ PLLA was measured by using a dynamic flow apparatus, and correlated by the lattice fluid theory of Sanchez and Lacombe. The results suggested that the value of having phase equilibrium data corresponding to morphology studies was the ability to calculate *S* and accurately describe where precipitation begins to take place in the nozzle. For the co-precipitation of PLLA and naproxen, PLLA microspheres (10-90 μm) loaded with naproxen and some free naproxen microparticles (1-5 μm) were observed at a pre-expansion *T* of 114 °C and an extraction *P* of 190 bar, and the composite particles consisted of a naproxen core surrounded by a thin polymer coating.

Songtipya et al [127] produce catechin/PLLA nanoparticles using RESOLV. The results showed that C_d, pre-expansion *T* and *P* had no significant effect on the shape and size of composite nanoparticles, which indicated that rapid expansion into a receiving solution effectively interrupted the collision and growth of particles in the

free jet. While, the *DL* and *EE* of catechin increased with increasing pre-expansion *T*, and with decreasing pre-expansion *P* and C_d. The effect of pre-expansion *T* and *P* could be explained by the degree of saturation (*s*) of catechin solutions, increasing pre-expansion *T* and decreasing pre-expansion *P* resulted in increasing *S* and hence a higher nucleation rate of catechin, as well as increased catechin precipitation and entrapment in PLLA along the expansion path. In addition, during rapid expansion, catechin tended to precipitate preferentially in the form of its own particles instead of being entrapped in PLLA with increasing C_d. However, different results were found by Sane et al [128], where asiatic acid/ PLLA nanoparticles were successfully produced by RESOLV, the results indicated that the *DL* and *EE* increased with increasing C_d/C_c, but decreased with increasing pre-expansion *T*.

Typical examples for PGSS co-precipitation/encapsulation processes are as follow. Rodrigues et al [129] obtained theophylline/HPO microcomposites by PGSS, the results showed that *P* had no significant effect on PS. However, particles shaped like needles, threads or fibers were more abundant at low pre-expansion *P*. Conversely, spheres were predominant at higher pre-expansion *P*. A reasonable explanation was proposed that at higher pre-expansion *P*, higher fluid densities are obtained and nucleation starts later in the expansion path. Dissolution studies showed that the Brophy and Deasy model was more adequate to follow the long-time drug dissolution kinetics for the HPO/theophylline system. However, a significant burst effect was observed because considerable amounts of theophylline were located at the particles surface.

de Paz E et al [130] encapsulated β-carotene in soybean lecithin using PGSS-drying technique. The influence of process variables on PS was correlated with the atomization process, which was enhanced by increasing the amount of CO_2 dissolved in the solution and the volumetric expansion ratio in the nozzle. The results also suggested that a basic requirement for a high *EE* was a good dispersion of the material to be encapsulated within the carrier matrix in the static mixer. If the pre-expansion *T* was increased, more water was extracted in the static mixer because the solubility of water in CO_2 increased with *T*, thus, the *EE* increased when the pre-expansion *T* was increased. Besides, with a concentrated solution of lecithin already formed in the static mixer, particles or oil droplets can more easily be surrounded by a shell of carrier material that can be mantained upon drying in the spray tower, leading to the prodution of microcapsules and an increase of the *EE*.

Typical examples for SAS co-precipitation/encapsulation processes are as follow.

Fraile et al [113] encapsulated quercetin in Pluronic F127 poloxamers by SAS process, the results suggested that for low-melting-*T* polymer, the particles were formed not by nucleation from the solution by the anti-solvent effect, but rather by solidification from a polymer melt. Although operation near the melting region was disadvantageous for the micronization of a pure polymer, it was a favorable condition for co-precipitation experiments, because it can facilitate the encapsulation of the active compound through the formation of a polymer film over active-component particles, avoiding the crystallization of segregated particles of active compound and polymer. The results also indicated that viable conditions for SAS co-precipitation of quercetin with Pluronic F127 were limited to a narrow range of C_d/C_c, in which quercetin particles can act as nucleation sites for the formation of polymer films. Further, formulations exhibited faster dissolution and a higher final solubility in simulated gastric and intestinal fluids, because of the morphological and structural properties conferred by SAS process.

Montes et al [131] co-precipitated Naproxen with Eudragit or PLLA by SAS process. For Naproxen-Eudragit systems, a larger PS was obtained with a lower *P*. This result can be explained by considering that an increase in *P* at constant *T* enhances the solvent power of $scCO_2$ toward the solvent, meaning that the liquid solvent molecules are more strongly captured by the CO_2, thus reducing the possible interaction between solvent, polymer and drug. The C_d/C_c had a negligible effect on PS but the *DL* was higher when a higher C_d/C_c ratio was used. The in vitro release profiles of the Naproxen-Eudragit and Naproxen-PLLA systems showed a slower and more controlled release in comparison to the untreated Naproxen.

Chen et al [132] prepared morphine-loaded PLLA and PLLA-PEG-PLLA microparticles by the SEDS process. Results showed that the actual *DL* increased with the increase of theoretical dosage while the *EE* decreased. The precipitated morphine particles might act as host particles, which lead to easy encapsulation of morphine by the precipitation of PLLA-PEG-PLLA particles. The 'soft' segment PEG grafted on the PLLA-PEG-PLLA made a great impact on the precipitation of microparticles, since the hydrophilicity of PEG and the increase of PEG content increased the solubility of copolymer in organic solvent. The release behaviors of microparticles varied greatly with the PEG content in the PLLA-PEG-PLLA copolymer, showing short-term release with burst release followed by sustained release within days or long-term release lasted for weeks.

Zabihi et al [133] successfully encapsulated nano-curcumin in poly(lactic-co-glycolic acid) through SAS-EM process, where poly(lactic-co-glycolic acid) solution was sprayed into $scCO_2$ media, in which nano-curcumin particles were fluidized by

ultrasonic vibration. The size and yielding of products decreased with increasing F_s. But the *DL* first decreases and then increases slightly. Ultrasonic power exhibited a crucial influence on microcapsules characteristics. Products had higher *DL* and higher yield with increasing ultrasonic power, which was owe to better mixing effects. In the other hand, higher ultrasonic power caused higher fluidization potential by which nano-curcumin was distributed more uniform in precipitation vessel, and resulted more efficient loading. High F_c also improved the *DL* and PSD when the ultrasonic power was high enough to prevent the particles being pulled out by net flow.

Besides, the effects of the various conditions on PS and PSD in SAS encapsulation process have been discussed in detail by Kalani et al [135]. The main factors for choosing the solvent and biodegradable polymer to produce fine particles to ensure effective drug delivery were emphasized and the effect of polymer structure on drug encapsulation was illustrated.

5. SUMMARY AND CHALLENGES

Major advances in drug delivery over recent years have highlighted the requirements of efficient methods for producing particles with designated microstructures. SCF processes, as a green and effective alternative to traditional method, have many advantages in particle design and show great potential in drug micronization and co-precipitation/encapsulation.

In this review, a theoretical framework of SCF PD is put forward for particular drug delivery, where the relationships among SCF processes, particle microstructures and performances are discussed in detail. Particle microstructures can be effectively tailored by controlling the operating parameters of SCF processes, where knowledge about the complicated mechanism of particle formation and growth is expected to help the screening and selection of suitable SCF process and its corresponding operating parameters. However, challenges and issues are still existed and need further study for the commercialization of SCF PD, such as following.

(a) Many researches have proved that the macroscopic properties of a drug delivery formulation are depend on the particle microstructures, however, it is still difficult to gain clear and definite requirements of a particular drug delivery on particle microstructures.

(b) Many different SCF processes have been developed and used for particle design, but it is difficult to choose a suitable SCF process for a particular drug delivery, because of the limited knowledge of complicated mechanism involved in SCF processes and insufficient fundamental solubility data of many drugs and/or

carrier materials in SCF.

(c) Although many of the nucleation and crystal growth mechanism and models involved in SCF processes have been proposed, it can only qualitatively predict the microstructures of the produced particles under different operating parameters, it is still difficult to get a quantitative prediction. Rational explanations and influence mechanisms of operating parameter on particle microstructures have been reported in most experimental studies. But in-depth thermodynamic and fluid dynamic study is not enough to determine a precise process path, and to screen and select the corresponding operating parameters.

(d) The industrialization of SCF PD processes have been considered and developed in recent years, but valid models or experience based on the experimental data are very limited to perform the scale-up of a pilot or industrial scale.

CONFLICT OF INTEREST

The authors confirm that this article content has no conflicts of interest.

ACKNOWLEDGEMENTS

Financial supports from the National Natural Science Foundation of China (Nos. 21276091, 21476086) and Ph.D. Programs Foundation of Ministry of Education of China (No. 20120172110010) are greatly appreciated.

ABBREVIATIONS

a, b	=	parameters of Peng-Robinson equation
ASES	=	Aerosol solvent extraction systems
c	=	mean thermal velocity
C_c	=	Carrier material concentration
C_d	=	Drug concentration
CFA	=	Cefuroxime axetil
CS	=	Chitosan
D	=	Droplet diameter
DCM	=	Dichloromethane
D_C	=	Diffusion coefficient
DDS	=	Drug delivery systems
DL	=	Drug loading
D_M	=	Diameter of the Mach disk

DMSO = Dimethyl sulfoxide

D_p = Diameter of the particles

D_{nozzle} = Nozzle diameter

D^T = Turbulent diffusivity

EOS = Equation of state

EtOH = Ethanol

e, A and B = parameters of Chrastil's equation

EE = Encapsulation efficiency

F = Vibration frequency

f = PEG mass fraction in PLLA-PEG-PLLA

FA = Folate

F_c = $scCO_2$ flow rate

F_s = Solution flow rate

G = Condensation growth rate

GAMA = Gas-assisted melting atomization

GAS = Gas antisolvent

HCPT = 10-Hydroxycamptothecin

PL = Proliposomes

HPO = Hydrogenated palm oil

IPA = Isopropyl alcohol

J = Nucleation rate

j_r = diffusive flux

k = turbulent kinetic energy

k_B = Boltzmann's constant

K_n = Knudsen number

LCEP = Lower critical end point

L_M = Length of the supersonic free jet region

L_{nozzle} = Length of the nozzle

M = Solvent molecular weight

MCP = Mixture critical point

MMPs = Magnetic microspheres

n = Particle size distribution function

N^* = Critical nuclei number concentration

P = Pressure

P_0 = Pre-expansion pressure

PCA = Precipitation with compressed antisolvent

PEG = Poly(ethylene glycol)

PF-RESS = Pre-filtration rapid expansion of supercritical solution

PLLA = Poly(lactic acid)

P_{post} = Expansion pressure

PR = Peng-Robinson

PS = Particle size

PSD = Particle size distribution

r = radial direction.

r^* = critical nucleus size

Re = Reynolds

RESOLV = Rapid expansion of supercritical solution into a liquid solvent

RESS = Rapid expansion of supercritical solution

RESS-N = Rapid expansion of supercritical solution with a non-solvent

RESS-SC = Rapid expansion of supercritical solution with solid cosolvent

S = Supersaturation

s = degree of saturation

S-L-V = Solid-Liquid-Vapor

SAS = Supercritical antisolvent

SAS-EM = Supercritical antisolvent with enhanced mass transfer

$ScCO_2$ = Supercritical CO_2

SCF = Supercritical fluids

SCF PD = Supercritical fluid particle design

SEDS = Solution enhanced dispersion by supercritical fluids

SEDS-PA = SEDS with prefilming atomization

T = Temperature

t = time

u = velocity

UCEP = Upper critical end point

v = volume

v^* = critical volume

v^S = solid molecular volume

w = mass fraction of DCM (or DCM + EtOH)

y = solute concentration

y_{eq} = saturation solute concentration

z	=	axial coordinate
α_c	=	condensation coefficient
β	=	Brownian coagulation coefficient
δ	=	standard Dirac function
ε	=	dissipation rate
κ	=	Zeldovich nonequilibrium factor
μ	=	viscosity
Θ	=	non-isothermal factor
ρ_1	=	density of supercritical fluids
σ	=	interfacial tension
τ_{jb}	=	time of jet break-up
τ_{stv}	=	time of surface tension vanishing
ω	=	mass fraction

REFERENCES

[1] Allen TM, Cullis PR. Drug delivery systems: entering the mainstream. Science 2004; 303: 1818-1822.

[2] Fahr A, Liu X. Drug delivery strategies for poorly water-soluble drugs. Expert Opin Inv Drug 2007; 4: 403-416.

[3] Loira-Pastoriza C, Todoroff J, Vanbever R. Delivery strategies for sustained drug release in the lungs. Adv Drug Deliver Rev 2014; 75: 81-91.

[4] Sun Y. Supercritical Fluid Particle Design for Poorly Water-soluble Drugs (Review). Curr Pharm Design 2014; 20:349-368.

[5] Jain KK. Drug delivery systems-an overview. In Jain KK (Ed), Drug Delivery Systems, Humana Press 2008: pp. 1-50.

[6] Rishikesh, Faruki MZ, Ghosh DR. Tailored Release Drug Delivery System (TRDDS), Int Res J Pharm App Sci 2012; 2: 128-137.

[7] Jain A, Bollinger JA, Truskett TM. Inverse methods for material design. AIChE J 2014; 00:1-9

[8] Aguilera JM. Why food microstructure?. J Food Eng 2005; 67: 3-11.

[9] York P. Strategies for particle design using supercritical fluid technologies. Pharm Sci Tech today 1999; 2: 430-440.

[10] Cansell F, Aymonier C. Design of functional nanostructured materials using supercritical fluids. J Supercrit Fluid 2009; 47: 508-516.

[11] Ginty PJ, Whitaker MJ, Shakesheff KM, et al. Drug delivery goes supercritical. Mater today 2005; 8: 42-48.

[12] Fages J, Lochard H, Letourneau JJ, et al. Particle generation for pharmaceutical applications using supercritical fluid technology. Powder Technol 2004; 141: 219-226.

[13] Elvassore N, Kikic I. Pharmaceutical processing with supercritical fluids. In: Bertucco A, Vetter G, Eds. High Pressure Process Technology: Fundamentals and Applications. Netherlands: Elsevier 2001; pp. 612-625

[14] Martín Á, Varona S, Navarrete A, et al. Encapsulation and co-precipitation processes with supercritical fluids: applications with essential oils. Open Chem Eng J 2010; 4: 31-41.
[15] Sekhon BS. Supercritical fluid technology: an overview of pharmaceutical applications. Int J Pharm Tech Res 2010; 2: 810-826.
[16] Tabernero A, Martín del Valle EM, Galán MA. Supercritical fluids for pharmaceutical particle engineering: Methods, basic fundamentals and modelling. Chem Eng Process 2012; 60: 9-25.
[17] Üner M, Yener G. Importance of solid lipid nanoparticles (SLN) in various administration routes and future perspectives. Int J Nanomed 2007; 2: 289.
[18] Rowland M. Influence of route of administration on drug availability. J Pharm Sci 1972; 61: 70-74.
[19] Shekunov BY, Chattopadhyay P, Tong HHY, Chow AHL. Particle size analysis in pharmaceutics: principles, methods and applications. Pharm Res 2007; 24: 203-227.
[20] Gaumet M, Vargas A, Gurny R, et al. Nanoparticles for drug delivery: the need for precision in reporting particle size parameters. Eur J Pharm Biopharm 2008; 69: 1-9.
[21] Desai MP, Labhasetwar V, Amidon GL, et al. Gastrointestinal uptake of biodegradable microparticles: effect of particle size. Pharm Res 1996; 13: 1838-1845.
[22] Kohli AK, Alpar HO. Potential use of nanoparticles for transcutaneous vaccine delivery: effect of particle size and charge. Int J Pharm 2004; 275: 13-17.
[23] Pilcer G, Amighi K. Formulation strategy and use of excipients in pulmonary drug delivery. Int J Pharm 2010; 392: 1-19.
[24] Fu Y, Kao WJ. Drug release kinetics and transport mechanisms of non-degradable and degradable polymeric delivery systems. Expert Opin Drug Del 2010; 7: 429-444.
[25] Langer R. New methods of drug delivery. Science 1990; 249: 1527-1533.
[26] Korsmeyer RW, Gurny R, Doelker EM, Buri P, Peppas NA. Mechanism of solute release from porous hydrophilic polymers. Int J Pharm1983; 15: 25-35.
[27] Dash S, Murthy PN, Nath L, et al. Kinetic modeling on drug release from controlled drug delivery systems. Acta Pol Pharm 2010; 67: 217-223.
[28] Mauger JW, Chilko D, Howard S. On the analysis of dissolution data. Drug Dev Ind Pharm1986; 12: 969-992.
[29] Polli JE, Rekhi GS, Augsburger LL, et al. Methods to compare dissolution profiles and a rationale for wide dissolution specifications for metoprolol tartrate tablets. J Pharm Sci 1997; 86: 690-700.
[30] Costa P, Lobo JMS. Modeling and comparison of dissolution profiles. Eur J Pharm Sci 2001; 13: 123-133.
[31] Papadopoulou V, Kosmidis K, Vlachou M, et al. On the use of the Weibull function for the discernment of drug release mechanisms. Int J Pharm 2006; 309: 44-50.
[32] Costa P. An alternative method to the evaluation of similarity factor in dissolution testing. Int J Pharm 2001; 220: 77-83.
[33] Shah VP, Tsong Y, Sathe P, et al. In vitro dissolution profile comparison-statistics and analysis of the similarity factor, f2. Pharm Res 1998; 15: 889-896.
[34] Bae YH, Park K. Targeted drug delivery to tumors: myths, reality and possibility. J Control Release 2011; 153: 198-205.
[35] Torchilin VP. Drug targeting. Europ Eur J Pharm Sci 2000; 11: S81-S91.

[36] Ruenraroengsak P, Cook JM, Florence AT. Nanosystem drug targeting: facing up to complex realities. J Control Release 2010; 141: 265-276.
[37] Florence AT, Halbert GW. Drug delivery and targeting. Phys Tech 1985; 16: 164-170.
[38] Farokhzad OC, Langer R. Impact of nanotechnology on drug delivery. ACS nano 2009; 3: 16-20.
[39] Perrut M, Clavier JY. Supercritical fluid formulation: process choice and scale-up. Ind Eng Chem Res 2003; 42: 6375-6383.
[40] Smith RD, inventor. Supercritical fluid molecular spray film deposition and powder formation. US Patent 4582731. 1986.
[41] Sane A, Limtrakul J. Formation of retinyl palmitate-loaded poly (l-lactide) nanoparticles using rapid expansion of supercritical solutions into liquid solvents (RESOLV). J Supercrit Fluid 2009; 51: 230-237.
[42] Young TJ, Mawson S, Johnston KP, et al. Rapid Expansion from Supercritical to Aqueous Solution to Produce Submicron Suspensions of Water-Insoluble Drugs. Biotechnol Progr 2000; 16: 402-407.
[43] Mishima K, Matsuyama K, Tanabe D, et al. Microencapsulation of proteins by rapid expansion of supercritical solution with a nonsolvent. AIChE J 2000; 46: 857-865.
[44] Thakur R, Gupta RB. Formation of phenytoin nanoparticles using rapid expansion of supercritical solution with solid cosolvent (RESS-SC) process. Int J Pharm 2006; 308: 190-199.
[45] Thakur R, Gupta RB. Rapid expansion of supercritical solution with solid cosolvent (RESS-SC) process: formation of griseofulvin nanoparticles. Ind Eng Chem Res 2005; 44: 7380-7387.
[46] Thakur R, Gupta RB. Rapid expansion of supercritical solution with solid cosolvent (RESS-SC) process: Formation of 2-aminobenzoic acid nanoparticle. J Supercrit Fluid 2006; 37: 307-315.
[47] Chiou AHJ, Yeh MK, Chen CY, et al. Micronization of meloxicam using a supercritical fluids process. J Supercrit Fluid 2007; 42: 120-128.
[48] Türk M. Manufacture of submicron drug particles with enhanced dissolution behaviour by rapid expansion processes. J Supercrit Fluid 2009; 47: 537-545.
[49] Weidner E, Knez Z, Novak Z, Inventors. A process and equipment for production and fractionation of fine particles from gas saturated solutions, World Patent WO 95/21688. 1994.
[50] Salmaso S, Elvassore N, Bertucco A, et al. Production of solid lipid submicron particles for protein delivery using a novel supercritical gas-assisted melting atomization process. J Pharm Sci 2009; 98: 640-650.
[51] Meterc D, Petermann M, Weidner E. Drying of aqueous green tea extracts using a supercritical fluid spray process. J Supercrit Fluid 2008; 45: 253-259.
[52] Gallagher PM, Coffey MP, Krukonis VJ, et al. Gas antisolvent recrystallization: new process to recrystallize compounds insoluble in supercritical fluids. In: Gallagher PM, Coffey MP, Krukonis VJ, Eds. Supercritical Fluid Science and Technology. Washington, DC: American Chemical Society 1989; pp.334-354.
[53] De la Fuente Badilla JC, Peters CJ, de Swaan Arons J. Volume expansion in relation to the gas-antisolvent process. J Supercrit Fluid 2000; 17: 13-23.
[54] Palakodaty S, York P, Pritchard J. Supercritical fluid processing of materials from aqueous

solutions: the application of SEDS to lactose as a model substance. Pharm Res1998; 15: 1835-1843.

[55] He W, Suo Q, Jiang Z H, et al. Precipitation of ephedrine by SEDS process using a specially designed prefilming atomizer. J Supercrit Fluid 2004, 31: 101-110.

[56] He W, Suo Q, Hong H, et al. Production of natural carotene-dispersed polymer microparticles by SEDS-PA co-precipitation. J Mater Sci 2007; 42: 3495-3501.

[57] Chattopadhyay P, Gupta RB. Production of griseofulvin nanoparticles using supercritical CO_2 antisolvent with enhanced mass transfer. Int J Pharm 2001; 228: 19-31.

[58] Pratsinis S E. Simultaneous nucleation, condensation, and coagulation in aerosol reactors. J Colloid Interf Sci 1988; 124: 416-427.

[59] Kalani A, Christofides P D. Simulation, estimation and control of size distribution in aerosol processes with simultaneous reaction, nucleation, condensation and coagulation. Comput Chem Eng 2002; 26: 1153-1169.

[60] Debenedetti PG. Homogeneous nucleation in supercritical fluids. AIChE J 1990; 36: 1289-1298.

[61] Friedlander S K, Ed. Smoke, Dust and Haze. New York: Oxford University Press, 2000.

[62] Gupta RB, Shim JJ. Solubility in supercritical carbon dioxide. USA: CRC Press 2006.

[63] Škerget M, Knez Z, Knez-Hrnčič M. Solubility of solids in sub-and supercritical fluids: a review. J Chem Eng Data 2011; 56: 694-719.

[64] Li J, Jin J, Zhang Z, et al. Equilibrium solubilities of a p-toluenesulfonamide and sulfanilamide mixture in supercritical carbon dioxide with and without ethanol. J Supercrit Fluid 2010; 52: 11-17.

[65] Jiang Y, Liu M, Sun W, et al. Phase Behavior of Poly (lactic acid)/Poly (ethylene glycol)/Poly (lactic acid)(PLA-PEG-PLA) in Different Supercritical Systems of CO_2+ Dichloromethane and CO_2+ C_2H_5OH+ Dichloromethane. J Chem Eng Data 2010; 55: 4844-4848.

[66] Ashour I, Almehaideb R, Fateen S E, et al. Representation of solid-supercritical fluid phase equilibria using cubic equations of state. Fluid Phase Equilibr 2000; 167: 41-61.

[67] Luo N, Lu Y, Jiang Y. Solubility of paclitaxel in mixtures of dichloromethane and supercritical carbon dioxide. Chinese J Chem Eng 2011; 19: 558-564.

[68] Li S, Varadarajan GS, Hartland S. Solubilities of theobromine and caffeine in supercritical carbon dioxide: correlation with density-based models. Fluid Phase Equilibr 1991; 68: 263-280.

[69] Sparks DL, Hernandez R, Estévez LA. Evaluation of density-based models for the solubility of solids in supercritical carbon dioxide and formulation of a new model. Chem Eng Sci 2008; 63: 4292-4301.

[70] Lucien FP, Foster NR. Solubilities of solid mixtures in supercritical carbon dioxide: a review. J Supercrit Fluid 2000; 17: 111-134.

[71] Kirby CF, McHugh MA. Phase behavior of polymers in supercritical fluid solvents. Chem Rev 1999; 99: 565-602.

[72] Elvassore N, Flaibani M, Bertucco A, et al. Thermodynamic analysis of micronization processes from gas-saturated solution. Ind Eng Chem Res 2003; 42: 5924-5930.

[73] Palakodaty S, York P. Phase behavioral effects on particle formation processes using supercritical fluids. Pharm Res 1999; 16: 976-985.

[74] Dixon DJ, Johnston KP, Bodmeier RA. Polymeric materials formed by precipitation with a

compressed fluid antisolvent. AIChE J 1993; 39: 127-139.
[75] Reverchon E, Caputo G, De Marco I. Role of phase behavior and atomization in the supercritical antisolvent precipitation. Ind Eng Chem Res 2003; 42: 6406-6414.
[76] Kayrak D, Akman U, Hortaçsu Ö. Micronization of ibuprofen by RESS. J Supercrit Fluid 2003; 26: 17-31.
[77] Hirunsit P, Huang Z, Srinophakun T, et al. Particle formation of ibuprofen-supercritical CO2 system from rapid expansion of supercritical solutions (RESS): A mathematical model. Powder Technol 2005; 154: 83-94.
[78] Helfgen B, Türk M, Schaber K. Theoretical and experimental investigations of the micronization of organic solids by rapid expansion of supercritical solutions. Powder technol 2000; 110: 22-28.
[79] Weber M, Russell LM, Debenedetti PG. Mathematical modeling of nucleation and growth of particles formed by the rapid expansion of a supercritical solution under subsonic conditions. J Supercrit Fluid 2002; 23: 65-80.
[80] Reverchon E, Pallado P. Hydrodynamic modeling of the RESS process. J Supercrit Fluid 1996; 9: 216-221.
[81] Martín A, Cocero MJ. Micronization processes with supercritical fluids: fundamentals and mechanisms. Adv Drug Deliver Rev 2008; 60: 339-350.
[82] Li J, Matos HA, Gomes de Azevedo E. Two-phase homogeneous model for particle formation from gas-saturated solution processes. J Supercrit Fluid. 2004; 32: 275-286.
[83] Li J, Rodrigues M, Paiva A, et al. Modeling of the PGSS process by crystallization and atomization. AIChE J 2005; 51: 2343-2357.
[84] Reverchon E, Torino E, Dowy S, et al. Interactions of phase equilibria, jet fluid dynamics and mass transfer during supercritical antisolvent micronization. Chem Eng J 2010; 156: 446-458.
[85] Martín A, Cocero M J. Numerical modeling of jet hydrodynamics, mass transfer, and crystallization kinetics in the supercritical antisolvent (SAS) process. J Supercrit Fluid 2004; 32: 203-219.
[86] Lengsfeld C S, Delplanque J P, Barocas V H, et al. Mechanism governing microparticle morphology during precipitation by a compressed antisolvent: atomization vs nucleation and growth. J Phys Chem B 2000; 104: 2725-2735.
[87] Reverchon E, Adami R, Caputo G, et al. Spherical microparticles production by supercritical antisolvent precipitation: interpretation of results. J Supercrit Fluid 2008; 47: 70-84.
[88] Reverchon E, De Marco I. Mechanisms controlling supercritical antisolvent precipitate morphology. Chem Eng J 2011; 169: 358-370.
[89] Reverchon E, De Marco I, Torino E. Nanoparticles production by supercritical antisolvent precipitation: a general interpretation. J Supercrit Fluid 2007; 43: 126-138.
[90] Reverchon E, De Marco I, Adami R, et al. Expanded micro-particles by supercritical antisolvent precipitation: interpretation of results. J Supercrit Fluid 2008; 44: 98-108.
[91] Rossmann M, Braeuer A, Dowy S, et al. Solute solubility as criterion for the appearance of amorphous particle precipitation or crystallization in the supercritical antisolvent (SAS) process. J Supercrit Fluid 2012; 66: 350-358.
[92] Dowy S, Torino E, Luther S K, et al. Imaging the supersaturation in high-pressure systems for particle generation. Chem Eng J 2011; 168: 896-902.

[93] Werling J O, Debenedetti P G. Numerical modeling of mass transfer in the supercritical antisolvent process. J Supercrit Fluid 1999; 16: 167-181.
[94] Chattopadhyay P, Gupta R B. Protein nanoparticles formation by supercritical antisolvent with enhanced mass transfer. AIChE J 2002; 48: 235-244.
[95] Topp M N. Ultrasonic atomization-a photographic study of the mechanism of disintegration. J Aerosol Sci 1973; 4: 17-25.
[96] Steckel H, Thies J, Müller B W. Micronizing of steroids for pulmonary delivery by supercritical carbon dioxide. Int J Pharm 1997; 152: 99-110.
[97] Todo H, Iida K, Okamoto H, et al. Improvement of insulin absorption from intratracheally administrated dry powder prepared by supercritical carbon dioxide process. J Pharm Sci 2003; 92: 2475-2486.
[98] Bakhbakhi Y, Charpentier P A, Rohani S. Experimental study of the GAS process for producing microparticles of beclomethasone-17, 21-dipropionate suitable for pulmonary delivery. Int J Pharm 2006; 309: 71-80.
[99] Keshavarz A, Karimi-Sabet J, Fattahi A, et al. Preparation and characterization of raloxifene nanoparticles using rapid expansion of supercritical solution (RESS). J Supercrit Fluid 2012; 63: 169-179.
[100] Varshosaz J, Hassanzadeh F, Mahmoudzadeh M, et al. Preparation of cefuroxime axetil nanoparticles by rapid expansion of supercritical fluid technology. Powder Technol 2009; 189: 97-102.
[101] Kim M S, Jin S J, Kim J S, et al. Preparation, characterization and in vivo evaluation of amorphous atorvastatin calcium nanoparticles using supercritical antisolvent (SAS) process. Eur J Pharm Biopharm 2008; 69: 454-465.
[102] Bolten D, Türk M. Micronisation of carbamazepine through rapid expansion of supercritical solution (RESS). J Supercrit Fluid 2012; 62: 32-40.
[103] Rossmann M, Braeuer A, Leipertz A, et al. Manipulating the size, the morphology and the polymorphism of acetaminophen using supercritical antisolvent (SAS) precipitation. J Supercrit Fluid 2013; 82: 230-237.
[104] Jiang Y, Sun W, Wang W. Recrystallization and micronization of 10-hydroxycamptothecin by supercritical antisolvent process. Ind Eng Chem Res 2012; 51: 2596-2602.
[105] Huang Z, Guo Y, Miao H, et al. Solubility of progesterone in supercritical carbon dioxide and its micronization through RESS. Powder Technol 2014; 258: 66-77.
[106] Dalvi S V, Azad M A, Dave R. Precipitation and stabilization of ultrafine particles of Fenofibrate in aqueous suspensions by RESOLV. Powder Technol 2013; 236: 75-84.
[107] Türk M, Bolten D. Formation of submicron poorly water-soluble drugs by rapid expansion of supercritical solution (RESS): results for naproxen. J Supercrit Fluid 2010; 55: 778-785.
[108] Lin P C, Su C S, Tang M, et al. Micronization of tolbutamide using rapid expansion of supercritical solution with solid co-solvent (RESS-SC) process. Res Chem Intermediat 2011; 37: 153-163.
[109] Chen W, Hu X, Hong Y, et al. Ibuprofen nanoparticles prepared by a PGSS™-based method. Powder Technol 2013; 245: 241-250.
[110] Esfandiari N, Ghoreishi S M. Synthesis of 5-Fluorouracil nanoparticles via supercritical gas antisolvent process. J Supercrit Fluid 2013; 84: 205-210.
[111] Xu J, Luo K Q. Enhancing the solubility and bioavailability of isoflavone by particle size

reduction using a supercritical carbon dioxide-based precipitation process. Chem Eng Res Des 2014; In Press.

[112] Yim J H, Kim W S, Lim J S. Recrystallization of Adefovir Dipivoxil Particles Using the Aerosol Solvent Extraction System Process. Ind Eng Chem Res 2014; 53: 1663-1671

[113] Fraile M, Buratto R, Gómez B, et al. Enhanced delivery of quercetin by encapsulation in poloxamers by supercritical antisolvent process. Ind Eng Chem Res 2014; 53: 4318-4327.

[114] Franceschi E, Kunita M H, Tres M V, et al. Phase behavior and process parameters effects on the characteristics of precipitated theophylline using carbon dioxide as antisolvent. J Supercrit Fluid 2008; 44: 8-20.

[115] Chang SC, Lee MJ, Lin H. The influence of phase behavior on the morphology of protein α-chymotrypsin prepared via a supercritical anti-solvent process. J. Supercrit Fluid 2008; 44: 219-229.

[116] Baseri H, Lotfollahi M N. Effects of expansion parameters on characteristics of gemfibrozil powder produced by rapid expansion of supercritical solution process. Powder Technol 2014; 253: 744-750.

[117] Liu G, Wang H, Jiang Y. Recrystallization and Micronization of Camptothecin by the Supercritical Antisolvent Process: Influence of Solvents. Ind Eng Chem Res 2013; 52: 15049-15056.

[118] Duarte A R C, Costa M S, Simplício A L, et al. Preparation of controlled release microspheres using supercritical fluid technology for delivery of anti-inflammatory drugs. Int J Pharm 2006; 308: 168-174.

[119] Lee L Y, Wang C H, Smith K A. Supercritical antisolvent production of biodegradable micro-and nanoparticles for controlled delivery of paclitaxel. J Control Release 2008; 125: 96-106.

[120] Wang W, Liu G, Wu J, et al. Co-precipitation of 10-hydroxycamptothecin and poly (l-lactic acid) by supercritical CO2 anti-solvent process using dichloromethane/ethanol co-solvent. J Supercrit Fluid 2013; 74: 137-144.

[121] Liu G, Wang W, Wang H, et al. Preparation of 10-hydroxycamptothecin proliposomes by the supercritical CO2 anti-solvent process. Chem Eng J 2014; 243: 289-296.

[122] Zu Y, Wang D, Zhao X, et al. A novel preparation method for camptothecin (CPT) loaded folic acid conjugated dextran tumor-targeted nanoparticles. Int J Mol Sci 2011; 12: 4237-4249.

[123] Zhao X, Jiang R, Zu Y, et al. Process optimization studies of 10-Hydroxycamptothecin (HCPT)-loaded folate-conjugated chitosan nanoparticles by SAS-ionic crosslink combination using response surface methodology (RSM). Appl Surf Sci 2012; 258: 2000-2005.

[124] Vezzù K, Campolmi C, Bertucco A. Production of lipid microparticles magnetically active by a supercritical fluid-based process. Int J Chem Eng 2009; 2009: 1-9.

[125] Chattopadhyay P, Gupta R B. Supercritical CO2 based production of magnetically responsive micro-and nanoparticles for drug targeting. Ind Eng Chem Res 2002; 41: 6049-6058.

[126] Chen A Z, Li L, Wang S B, et al. Study of Fe3O4-PLLA-PEG-PLLA magnetic microspheres based on supercritical CO2: Preparation, physicochemical characterization, and drug loading investigation. J Supercrit Fluid 2012; 67: 139-148.

[127] Songtipya L, Sane A. Effect of concentration and degree of saturation on co-precipitation of catechin and poly (l-lactide) by the RESOLV process. J Supercrit Fluid 2013; 75: 72-80.
[128] Sane A, Limtrakul J. Co-precipitation of asiatic acid and poly (l-lactide) using rapid expansion of subcritical solutions into liquid solvents. J Nanopart Res 2011; 13: 4001-4013.
[129] Rodrigues M, Peiriço N, Matos H, et al. Microcomposites theophylline/hydrogenated palm oil from a PGSS process for controlled drug delivery systems. J Supercrit Fluid 2004; 29: 175-184.
[130] de Paz E, Martín Á, Cocero M J. Formulation of β-carotene with soybean lecithin by PGSS (Particles from Gas Saturated Solutions)-drying. J Supercrit Fluid 2012; 72: 125-133.
[131] Montes A, Kin N, Gordillo M D, et al. Polymer-naproxen precipitation by supercritical antisolvent (SAS) process. J Supercrit Fluid 2014; 89: 58-67.
[132] Chen F, Yin G, Liao X, et al. Preparation, characterization and in vitro release properties of morphine-loaded PLLA-PEG-PLLA microparticles via solution enhanced dispersion by supercritical fluids. J Mater Sci 2013; 24: 1693-1705.
[133] Zabihi F, Xin N, Li S, et al. Polymeric coating of fluidizing nano-curcumin via anti-solvent supercritical method for sustained release. J Supercrit Fluid 2014; 89: 99-105.
[134] Kim J H, Paxton T E, Tomasko D L. Microencapsulation of naproxen using rapid expansion of supercritical solutions[J]. Biotechnol Progr 1996; 12: 650-661.
[135] Kalani M, Yunus R. Application of supercritical antisolvent method in drug encapsulation: a review. Int J Nanomed 2011; 6: 1429-1442.

Tables

Table 1. The most common administration methods and their advantages and disadvantages

Methods	Advantage	Disadvantage
Oral administration	• The preferred route • Easy administration • Widespread acceptance	• Low bioavailability • Gastrointestinal tract problems • Not suitable for drugs targeted
Injection	• Rapid onset of action • Predictable bioavailability • Avoidance gastrointestinal tract	• Pain involved and patient compliance • Dangerous medical waste • Disease transmission by needle reuse
Transdermal administration	• Non-invasive • Long release periods • Improved patient compliance	• Significant barrier properties of skin • Only a limited number of drugs are amenable to administration
Pulmonary drug delivery	• Large absorption surface area • Avoidance of the first pass hepatic metabolism • High therapeutic effects	• Drug deposition • Deposited particles cleared by the mucous toward the throat • High demands on the inhalation devices

Table 2. Summary of the SCF PD processes and their mainly operating parameters

Role of SCF	Process	Modifications	Mainly operating parameters
Solvent	RESS	RESSOLV RESSAS RESS-N RESS-SC PF-RESS	Extraction T and P CO_2 flow rate (F_c) Solution flow rate (F_s) Pre-expansion T and P Expansion T Nozzle design
Solute	PGSS	GAMA PGSS-drying	Operating T and P F_c and F_s Nozzle design CO_2/solute ratio
Antisolvent	SAS	GAS PCA/ASES SEDS SEDS-PA SAS-EM	Organic solvent Drug concentration (C_d) Carrier material concentration (C_c) Nozzle design F_c and F_s T and P

Table 3. Examples of SCF micronization processes

Drug/Method	Operating parameters	Results	Ref.
Progesterone/ RESS	Extraction *T*: 40-60 ºC Extraction *P*:120-260 bar D_{nozzle}: 60-350 µm	PS: 150 µm to 0.11-3.22 µm PS decreases with D_{nozzle} increases, but increases with extraction *P* or *T*.	[105]
Fenofibrate/ RESOLV	Pre-expansion *P*:100-200 bar D_{nozzle}:127-762 µm L_{nozzle}:3-6 cm 8 different stabilizers	PS: 0.5-5 µm Stabilizers have a great effect on particle properties	[106]
Naproxen/ RESS and RESSAS	Extraction *P*: 200-300 bar Pre-expansion *T*: 50-90 ºC Pre-expansion *P*: 200-300 bar	PS: 0.56-0.82 µm (RESS) and 0.3 µm (RESSAS) RESSAS can effectively minimize particle growth	[107]
Tolbutamide/ RESS and RESS-SC	Extraction *T*: 35-45 ºC Extraction *P*: 150-200 bar Pre-expansion *T*: 120 ºC Solid co-solvent: Menthol	PS: 8.5-9.2 µm (RESS) and 2.1- 2.9 µm (RESS-SC) The polymorph conversion from form I to form II	[108]
Ibuprofen/ PGSS	Operating *P*: 100-250 bar Operating *T*: 50-80 ºC F_s :1.0 -3.2 ml/min Dispersing matrices: PEG2000 - PEG6000	PS: 20-500 nm PS decreases with *P* and molecular weight of PEG increases, but increases with *T* or F_s.	[109]
5-Fluorouracil / GAS	*T*: 34-46 ºC *P*: 90-150 bar C_d: 20-100 mg/mL F_s:1.6-2.4 mL/min	PS:260-600 nm PS decreased with decreasing *T* and C_d and with increasing *P* and F_s	[110]
Isoflavone/ PCA	*P*: 85-120 bar C_d: 0.4-4 mg/mL Solvent: Acetone, EtOH, EtOH+ Acetone	PS: 10-50 µm to 254 nm at width Reduction PS increased 2 fold water solubility and improved 2.6 fold plasma concentration after oral administration in rat	[111]
Adefovir Dipivoxil/ ASES	*T*: 28-50 ºC, P: 70-200 bar F_s: 0.2-1 mL/min C_d: 0.5-2 wt% Solvent: ethanol, methanol , and isopropyl alcohol (IPA)	PS decreases with decreased *T*, C_d and F_s, and with increased *P*. The order of solvents was methanol < ethanol < IPA	[112]
Quercetin/ SEDS	*T*: 35-45 ºC, *P*: 100-200 bar F_s: 1-5 mL/min Flow time: 4-20 min C_d: 5-10 mg/mL Ultrasonic power:100-300 W	PS: 47.4 µm to 0.12-0.45µm PS decreases with increasing F_s and ultrasonic power, decreasing drug C_d and flow time	[113]

Table 4. Examples of SCF co-precipitation/encapsulation processes

Drug/ Carrier material	Method	Operating parameters	Results	Ref.
Catechin/ PLLA	RESOLV	C_d: 0.1-0.2 wt%, C_c: 0.2 wt% Pre-expansion *T*: 60-100 °C Pre-expansion *P*:265-325 bar D_{nozzle}: 60-350 μm	PS: 30-40 nm *DL*: 2.4-7.3% *EE*: 4.7-22.0%	[127]
Asiatic acid/ PLLA	RESOLV	C_c: 0.2-0.4 wt% C_d/C_c:1:2-1:4 Pre-expansion *T*: 70-100 °C Pre-expansion *P*: 330 bar	PS: 50-54 nm *DL*: 7.6-20.7% *EE*: 37.8-62.2%	[128]
Theophylline / HPO	PGSS	Mixing *T*: 60 °C Mixing *P*: 120-180 bar Pre-expansion *T*: 86 °C F_c: 0.18-1.25 g min−1	PS: 2.5-3.0 μm *DL*: 0.5 -3.5%	[129]
β-carotene/ soybean lecithin	PGSS-drying	C_c: 55 -72 g/L Operating *T*: 100-130 °C Operating *P*: 80-100 bar F_c / F_s: 21- 37 g/g	PS: 10-500 μm Rehydration PS: 1-5 μm *EE*: 29-60%	[130]
Quercetin/ Pluronic F127	SAS	C_d: 0.01-0.02 g/mL C_d/C_c: 2:1-1:9 Solvent: acetone	*DL*: 35-56% The PS and morphology are conferred	[113]
Naproxen/ Eudragit or PLLA	SAS	*P*: 100-200 bar *T*: 40-50 °C Content of PEG: 0-5% C_d: 5-8 mg/mL C_d/C_c: 1:1-1:5	Naproxen/Eudragit PS: 0.56-1.43μm *DL*: 3.0-13.2% Naproxen/ PLLA PS: 0.08-0.31 μm *DL*: 4.5-25.6%	[131]
Morphine/ PLLA-PEG-PLLA	SEDS	*P*: 80-140 bar, *T*: 35 °C Content of PEG: 0-5% C_d: 4-12 mg/mL C_d/C_c: 1:5-1:10	PS: 2.04-5.73μm *DL*: 8.3-17.9% *EE*: 51.8-79.0%	[132]
Curcumin/ PLGA	SAS-EM	*P*: 80-100 bar, *T*: 23-38 °C F_s: 1.0-2.5 mL/min Power: 100-180 W Solvent: Acetone, Acetone + EtOH, EthylAcetate + EtOH	PS: 40-1680 nm *DL*: 4-38% PS and *DL* can be enhanced by increasing ultrasound power	[133]

Figures

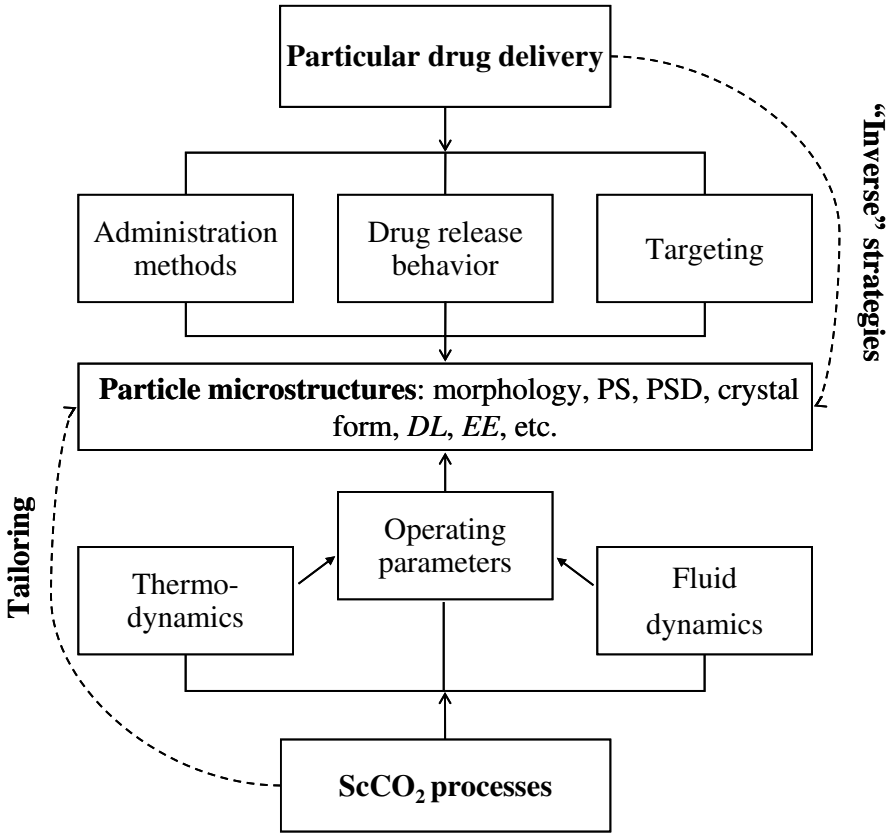

Fig. 1. An overall view of SCF PD for particular drug delivery.

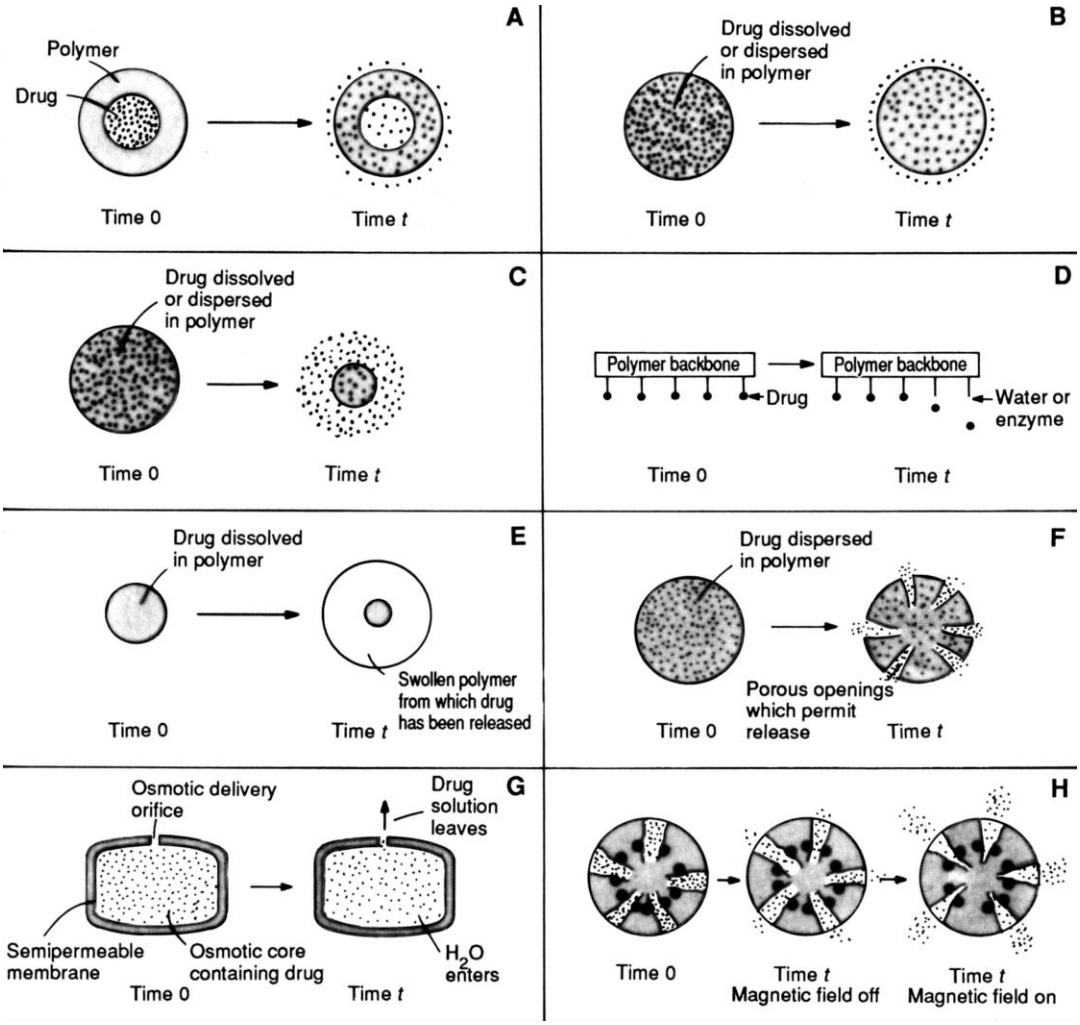

Fig. 2. Drug release mechanisms from a polymeric material [25].

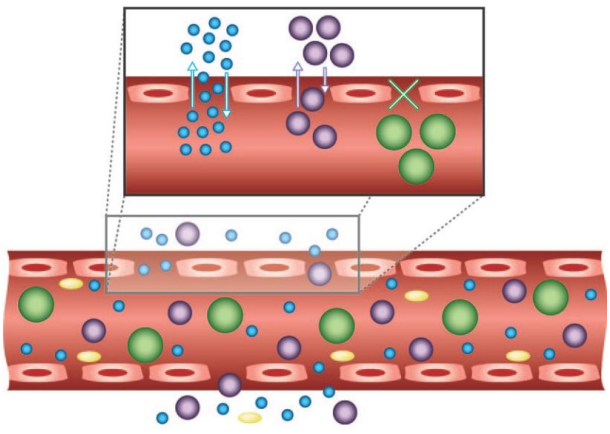

Fig. 3. Requirements of particle uptake on surface properties [38].

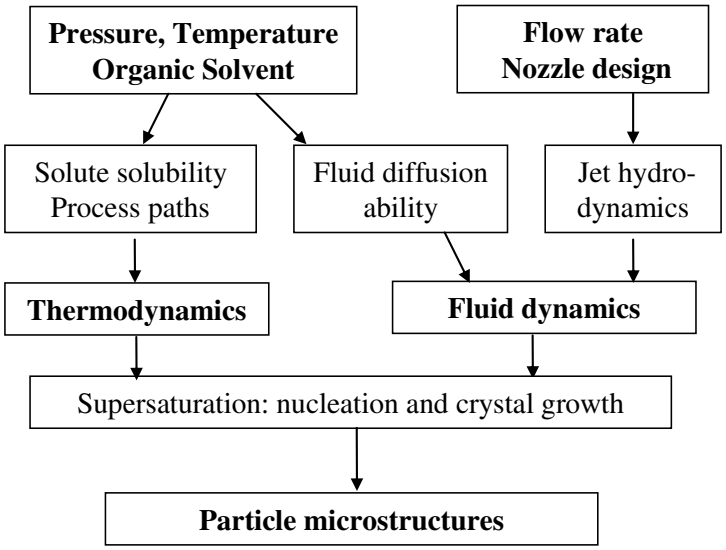

Fig. 4. Influencing mechanism of operating parameters on particle microstructures

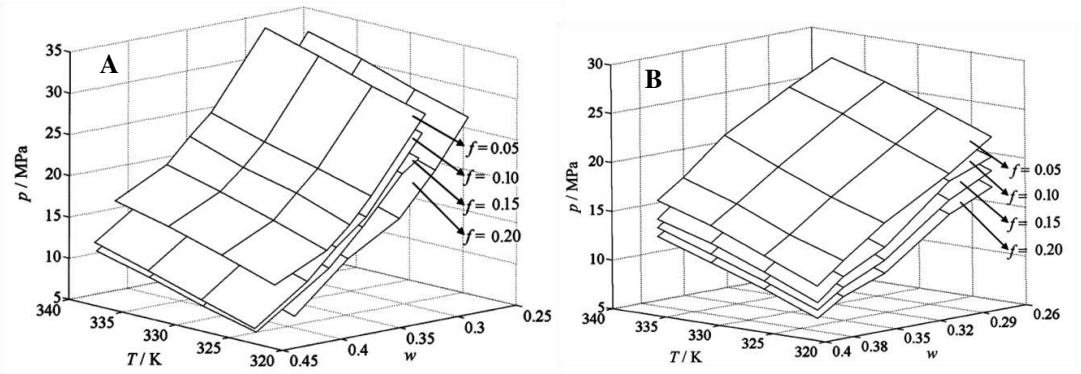

Fig. 5 *P-T-w* space diagram of PLA-PEG-PLA in (A) CO_2 + DCM system and (B) CO_2 + DCM + C_2H_5OH system [65].

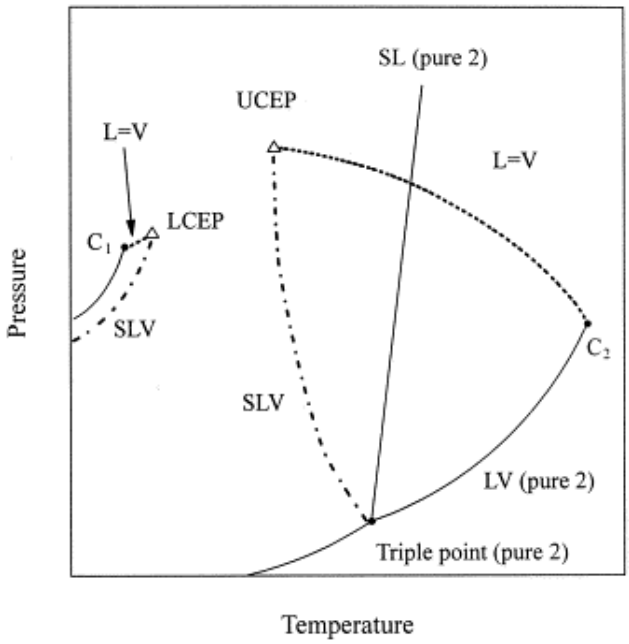

Fig. 6. Typical phase diagram for an asymmetric binary mixture consisting of a solid (component 2) and CO_2 (component 1) at high P [70].

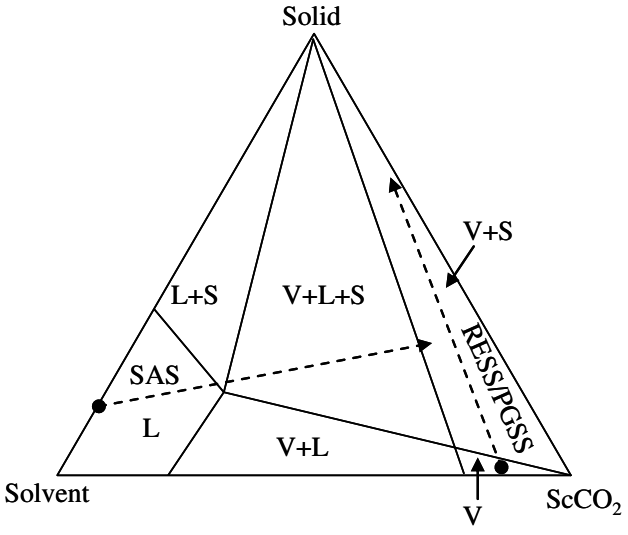

Fig. 7. A simple representative phase diagram of the ternary solid-solvent-scCO_2 systems at constant T and P.

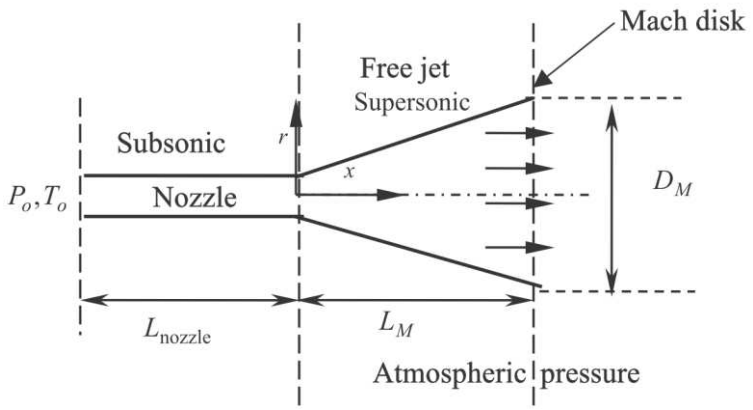

Fig. 8. A schematic of the RESS expansion device [77].

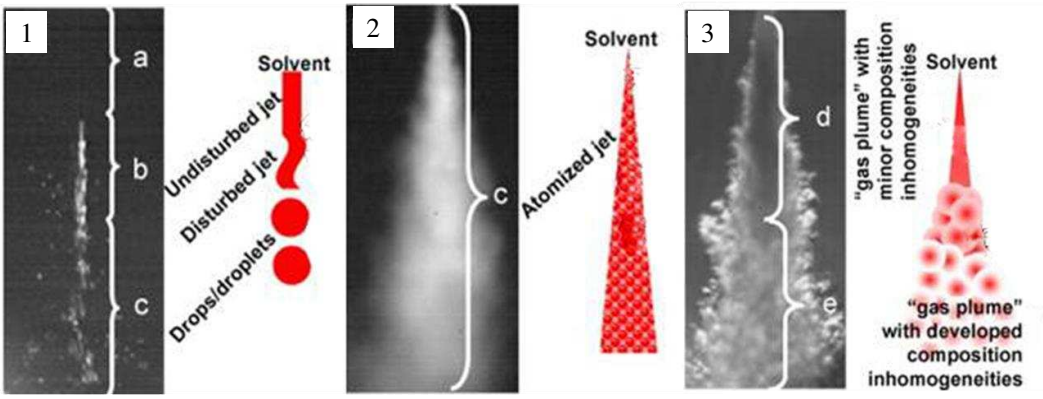

Fig. 9. Scattering phenomena related to SAS jet mixing [84].

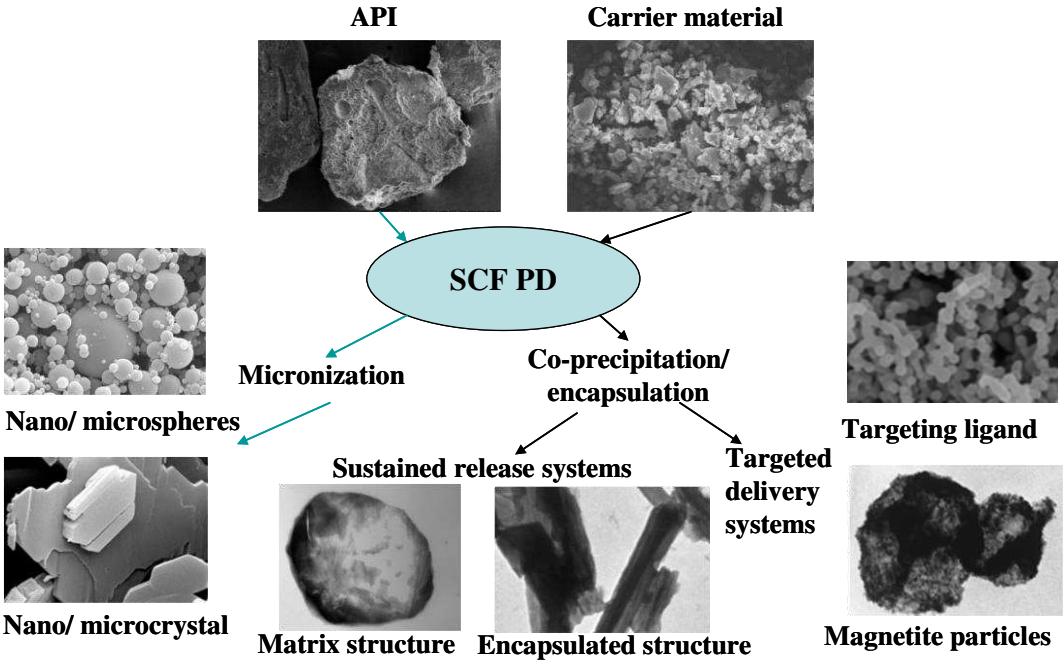

Fig. 10. The typical SCF PD processes for particular drug delivery

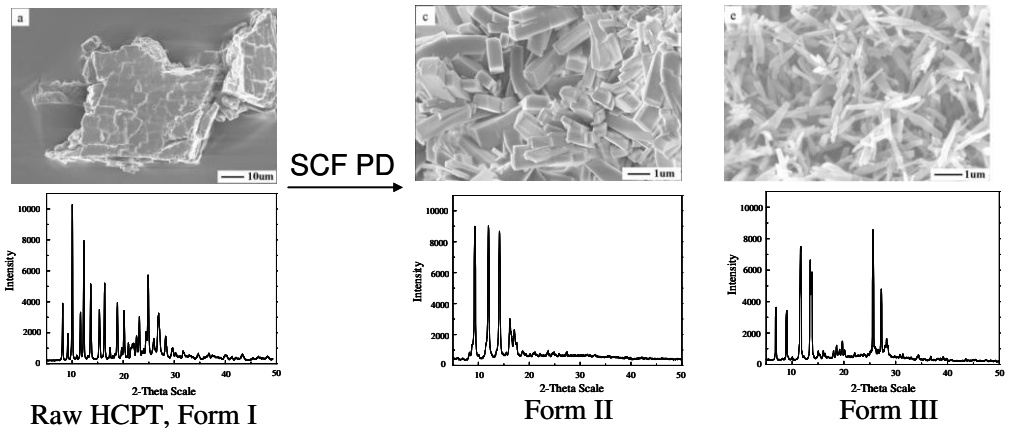

Fig. 11. SEM and XRD of unprocessed and SAS processed HCPT [104].

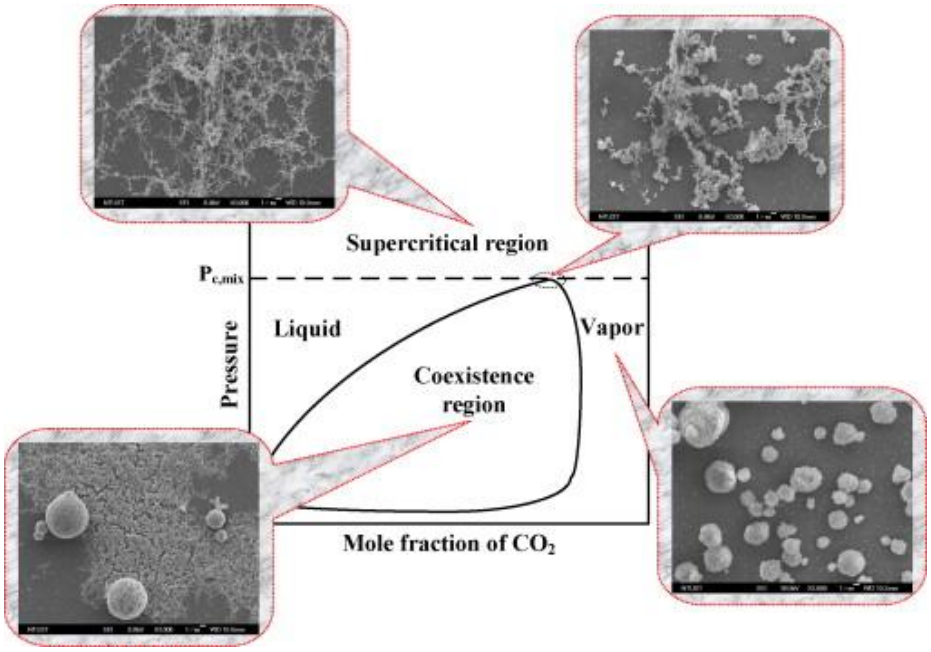

Fig. 12. SEM images of α-chymotryps in particulate samples prepared from different phase regions [115].

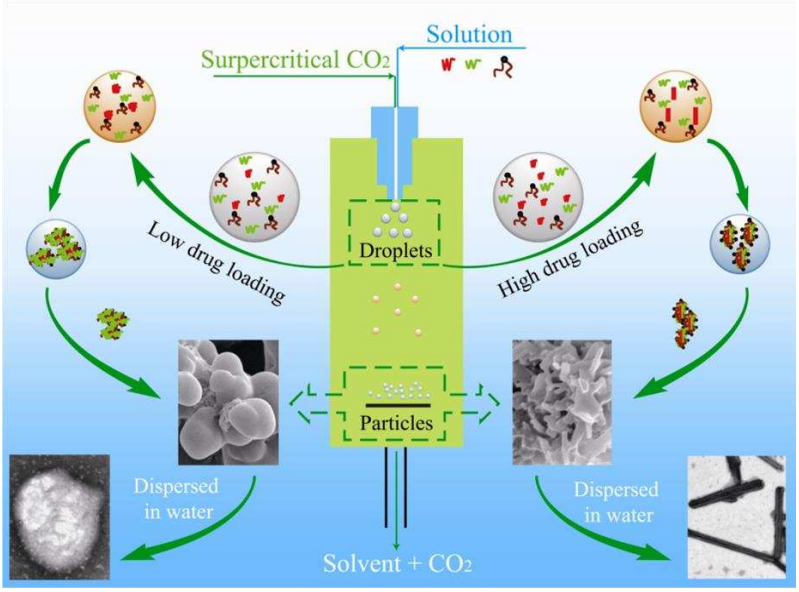

Fig. 13. Schematic representation of obtained spherical or clavate HCPT-PL under different drug loading.